



# Enhancing the understanding of surfactant influence in LTA crystallization through microwave-assisted methods at different temperatures

Dilini Perera<sup>1</sup> · Lasanga Amarasena<sup>1</sup> · Venura Madhusanka<sup>2</sup> · Xing Chen<sup>3</sup> · Rohan Weerasooriya<sup>1</sup> · Athula Bandara<sup>2</sup> · Lakmal Jayarathna<sup>1</sup>

Accepted: 31 December 2024

© The Author(s), under exclusive licence to Springer Science+Business Media, LLC, part of Springer Nature 2025

## Abstract

Achieving specific framework structures and morphologies in zeolite synthesis is crucial for broad applications. This study addresses the limited understanding of surfactant effects on crystal imperfections and phase purity in LTA zeolite synthesis, particularly under microwave-assisted conditions. We hypothesized that anionic, cationic, and non-ionic surfactants would significantly affect phase purity, morphology, crystallite size, and imperfections in LTA zeolites synthesized at varying microwave temperatures. Synthesized materials were characterized using powder X-ray diffraction, scanning electron microscopy (SEM), Raman spectroscopy, and Fourier transform infrared (FTIR) spectroscopy. Findings revealed that within the 100–150 °C microwave temperature range, all surfactants primarily yielded the LTA-type zeolite structure. However, a metastable phase was observed in materials synthesized at 130 °C with Sodium Dodecyl Sulfate (SDS), as indicated by reduced crystallinity and an additional Raman peak at 471 cm<sup>-1</sup>. This suggests that while the LTA framework remained predominant, symmetry disturbances at this temperature impacted TO<sub>4</sub> stretching vibrations, possibly leading to a partial deviation from phase purity. Surfactants significantly influenced phase purity, morphology, crystallite size, and crystal imperfections, with optimal phase purity achieved at lower temperatures (100–110 °C) for anionic and non-ionic surfactants and at higher temperatures (130–150 °C) for cationic surfactants. Crystallite sizes varied in a complex, temperature-dependent manner, suggesting further investigation into crystallization mechanisms. An inverse correlation between microstrain and crystallite size was observed across samples, except at 130 °C, likely due to added stress and supplementary crystal phases. This study establishes foundational knowledge for selecting surfactants to modify pore structures in hierarchical LTA zeolites and offers insights for designing LTA zeolites with tailored properties, addressing knowledge gaps, and advancing zeolite synthesis techniques.

---

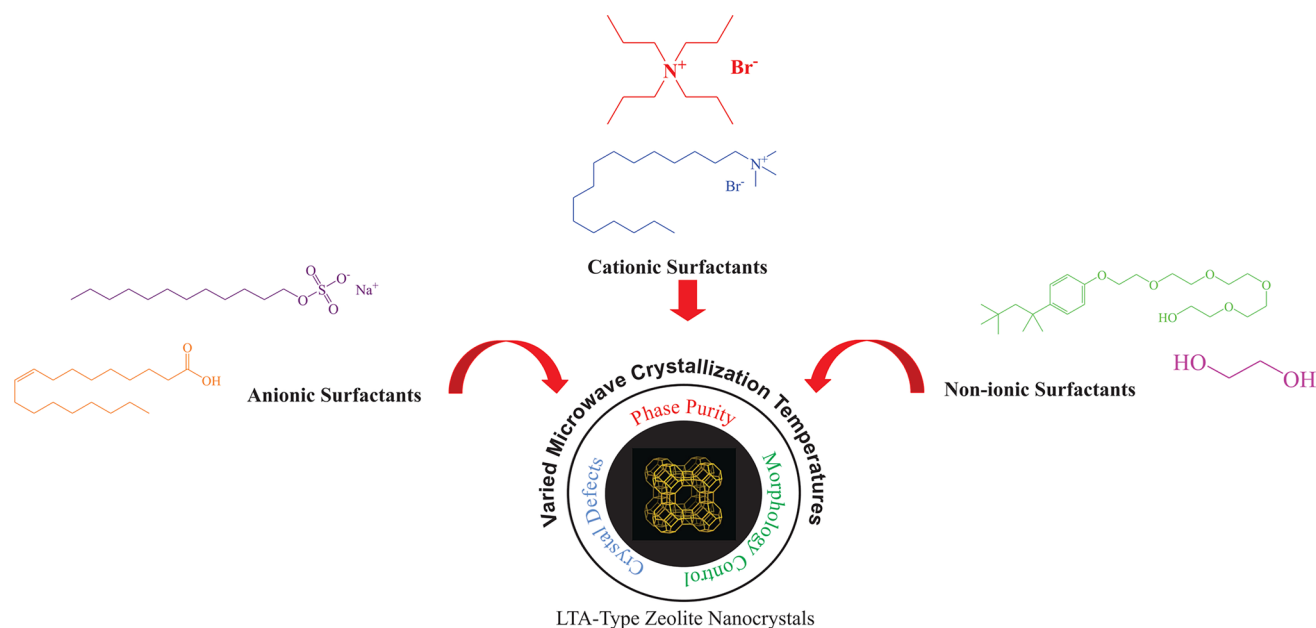
✉ Lakmal Jayarathna  
lakmal.ja@nifs.ac.lk

<sup>1</sup> National Institute of Fundamental Studies, Hantana, Kandy, Sri Lanka

<sup>2</sup> Department of Chemistry, Faculty of Science, University of Peradeniya, Kandy, Sri Lanka

<sup>3</sup> Institute of Industry and Equipment Technology, Hefei University of Technology, Hefei 230009, China

## Graphical abstract



**Keywords** Crystal defects · LTA zeolite · Phase purity · Structure-modifiers · Surfactants

## 1 Introduction

Zeolites are microporous crystalline aluminosilicates, which exist naturally (as minerals) and can be synthesized in laboratories with different chemical compositions, pore topologies, and/or crystal sizes. The International Zeolite Association (IZA) database shows that around 250 such zeolitic structural types with unique framework topologies have been reported so far, thanks to the development of successful synthetic techniques [1]. Owing to this large versatility, zeolites have been utilized in a wide range of applications, including gas adsorption and separation [2], as catalysts [3], petrochemistry [4], biotechnological and medicinal applications [5], and so on.

Synthesizing zeolites with specific framework structures and desired morphology is a complex endeavor, yet essential due to the direct influence of these properties on their unique applications [6]. Achieving these specific characteristics often requires careful selection of synthesis conditions and parameters such as reactant composition, pH of the gel, aging conditions, crystallization temperature, and duration [7]. However, in cases where these conditions alone cannot yield the desired structures, additives play a crucial role. These additives include metal cations, metal complexes, organic amines, organic quaternary ammonium bases, and inorganic salts. They act as structure-directing agents (SDAs) or templates, effectively

directing the framework structure of the zeolite towards the desired form. By residing within the cavities, they facilitate the formation of specific geometric configurations and structures during the nucleation stage and subsequently stabilize these structures [8]. Among several types of templates/SDAs, surfactants are of much interest, and surfactant-templating is reported as one of the most effective synthetic strategies for designing well-defined porous materials like zeolites [9].

Zeolite A, among the most commonly used synthetic zeolites, has been employed across a range of industrial sectors. Zeolite A possesses a Linde Type A (LTA) structure according to the IZA. Primarily utilized in its sodium form (4A), its dehydrated chemical composition is represented by  $[\text{Na}_{12}^+(\text{H}_2\text{O})_{27}]_8[\text{Al}_{12}\text{Si}_{12}\text{O}_{48}]_8$  [10]. Linde Type A (LTA) zeolites can indeed be synthesized without the assistance of SDAs. However, there are instances where SDAs are employed, especially in the synthesis of high-silica ( $\text{Si}/\text{Al} > 5$ ) and pure-silica LTA variants, highlighting the ongoing demand for various SDAs in LTA synthesis. Sun et al. reported a study where 4-methyl-2,3,6,7-tetrahydro-1H,5H-pirido[3,2,1-ij]-quinolinium used as a dynamic structure-directing agent at different concentrations in synthesizing pure-silica LTA and one of its closely competing zeolite type, pure-silica AST zeolite [11]. Furthermore, Schmidt et al. reported that the use of triquatery organic structure-directing agents can promote the formation of LTA zeolite in the germanosilicate or aluminophosphate reaction pathways

[12]. Therefore, it is evident that there remains a significant demand for various SDAs in the synthesis of LTA zeolite variants.

Another significant aspect of LTA zeolite synthesis is the use of surfactants as pore-modifiers in the synthesis of mesoporous and hierarchical LTA. For example, studies reported by Cho et al. and Feng et al. demonstrate the ability of organosilane surfactants respectively, [3-(trimethoxysilyl)propyl]-hexadecyl-dimethylammonium chloride [13] and [3-(trimethoxysilyl)propyl]-tetradecyl-dimethylammonium chloride [14] in mesopore generation in LTA zeolite crystallization process. The most prominent finding of these studies was that organosilane surfactants in the gels had a significant impact on LTA phase crystallization in addition to mesopore formation, even though its role as an SDA had not been considered. Surfactant concentration significantly affected changes in LTA crystal properties, indicating that mesopores within the LTA zeolite may have induced imperfections in the LTA single crystals owing to surfactant presence [14]. This implies the necessity of comprehensively evaluating the influence of surfactants on the crystal properties of LTA when surfactants are used as modifiers. Almost all the reported research studies related to this have generally investigated the structural and morphological characteristics of resulting LTA [15, 16]. However, investigations into how the crystal imperfections and LTA phase purity vary with different types of surfactants are not completely addressed. Recently, research efforts have been made to rationally synthesize zeolites with tunable porous properties using potential modifiers [17, 18]. Identifying additional surfactants that could serve as effective modifiers during LTA synthesis, without inducing phase transformations or defect formation, and ensuring a higher phase purity, is crucial before their consideration for pore-modifying studies. Another fact is that in the last decade, microwave-assisted crystallization has been widely used since it offers advantages over conventional hydrothermal synthesis such as high phase purity and short crystallization time [19]. Kannagara, et al. reported that the microwave approach was more effective in the microwave-assisted LTA synthesis over hydrothermal, when the anionic surfactant, SDS was employed as a particle size-controlling agent. However, they indicate that lower aging temperatures can lead to the formation of crystal phases such as sodalite [20]. This highlights the need to further investigate the influence of aging and crystallization temperatures on the resulting properties of LTA such as phase purity and the possibility of phase transformations in the presence of different surfactants.

To address the aforementioned knowledge gaps, we present a fundamental study aimed at understanding the effects of the presence of different anionic, cationic, and non-ionic surfactants on the properties of LTA zeolite during microwave crystallization. To the best of our knowledge, this is

the first time such an investigation has been presented and specifically, we focused on studying the variations in resulting properties of LTA such as phase purity, crystal imperfections, crystallite size, and phase transformations in a range of crystallization temperatures. We believe this knowledge will serve as a crucial foundation for future research, guiding the selection of surfactants for synthesizing hierarchical and mesoporous LTA using surfactants as pore modifiers, synthesis of LTA variants such as high-silica and pure-silica zeolites using surfactants as structure-directing agents, as well as for the rational synthesis of LTA zeolites with tailored properties. Overall, this study not only fills critical gaps in current knowledge but also provides a solid basis for future advancements in the synthesis and customization of LTA zeolites for specific applications.

## 2 Experimental section

### 2.1 Material synthesis

All the chemicals for zeolite synthesis were obtained from Sigma-Aldrich and used as received unless otherwise mentioned. Mainly, Sodium aluminate ( $\text{NaAlO}_2$ ) (As Alumina source), Sodium metasilicate ( $\text{Na}_2\text{SiO}_3 \cdot 5\text{H}_2\text{O}$ ) (As silica source), Sodium Hydroxide ( $\text{NaOH}$ ), and surfactants; SDS ( $\text{CH}_3(\text{CH}_2)_{11}\text{OSO}_3\text{Na}$ ), Oleic acid, Tetrapropylammonium bromide (TPAB) and Hexadecyltrimethylammonium bromide (HDAB), Triton, and polyethylene glycol (PEG) were used for the synthesis process. Deionized water (DI) was used in all cases.

A modified microwave synthesis method [20] was used to synthesize LTA in the presence of surfactants (Fig. 1). A hydrogel with a molar ratio of 4.0  $\text{SiO}_2$ :1.0  $\text{Al}_2\text{O}_3$ :5.5  $\text{Na}_2\text{O}$ :190  $\text{H}_2\text{O}$  was used. Microwave heating was used for zeolite crystallization and anionic (SDS and Oleic acid), cationic (TPAB and HDAB), and non-ionic (Triton and PEG) surfactants were used as the different types of surfactants. Samples synthesized in the presence of SDS, Oleic acid, TPAB, HDAB, Triton, and PEG at 100, 110, 130, and 150 °C temperatures have called as SDS-100, SDS-110, SDS-130, SDS-150, Oleic-100, Oleic-110, Oleic-130, Oleic-150, TPAB-100, TPAB-110, TPAB-130, TPAB-150, HDAB-100, HDAB-110, HDAB-130, HDAB-150, Triton-100, Triton-110, Triton-130, Triton-150, PEG-100, PEG-110, PEG-130, PEG-150, respectively in this paper. Initially, 50 mL of  $\text{NaOH}$  solution was prepared by adding the required amount of  $\text{NaOH}$  to DI water. 2.42 g of  $\text{NaAlO}_2$  was added to the above mixture under continuous stirring to obtain a clear solution. Then, 10 mL of a 1 M surfactant solution was added to the above solution, followed by the addition of  $\text{Na}_2\text{SiO}_3 \cdot 5\text{H}_2\text{O}$  under vigorous stirring. The obtained homogeneous gel solution was allowed to age for

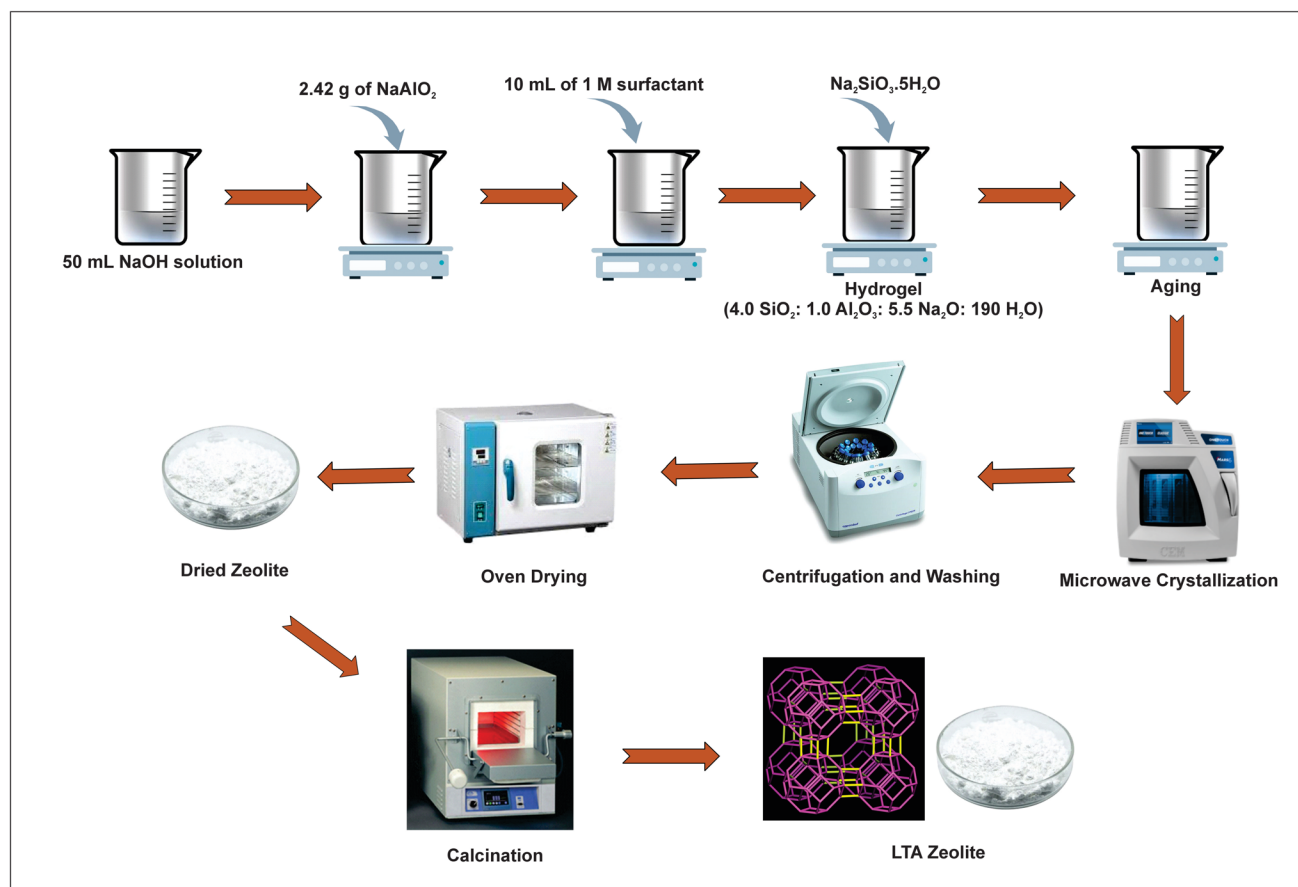


**Fig. 1** Graphical interpretation of the methodology for synthesizing LTA-type zeolite in the presence of various surfactants and crystallization temperatures

a certain time. Microwave heating was then carried out with 900 W for 3 h (the MARS 6 Microwave Digestion System was used) at varying crystallization temperatures (100, 110, 130, and 150 °C). Thereafter, the product was isolated by filtration, washed with DI water, dried, and calcinated at 550 °C for 5 h.

## 2.2 Material characterization

PXRD characterization was performed in a diffractometer (Rigaku Ultima IV, Japan) at 20 kV and 30 mA using Cu-K $\alpha$  radiation at  $\lambda = 0.154$  nm. Data were collected in the step scanning mode within the two  $\theta$  angles of 0° to 90°. The surface morphology of synthesized zeolites was analyzed using scanning electron microscopy (SEM ZEISS EVO 15 detector). A thin layer of gold is deposited onto the non-metallic samples to improve conductivity. The samples were thoroughly dried before being placed in a high-vacuum environment for the analysis. For the Raman spectroscopic characterization, the Raman spectrometer (RENISHAW, UK) was used in the 100 to 3200  $\text{cm}^{-1}$  range with a 514 nm laser excitation. For the FTIR characterization of zeolite

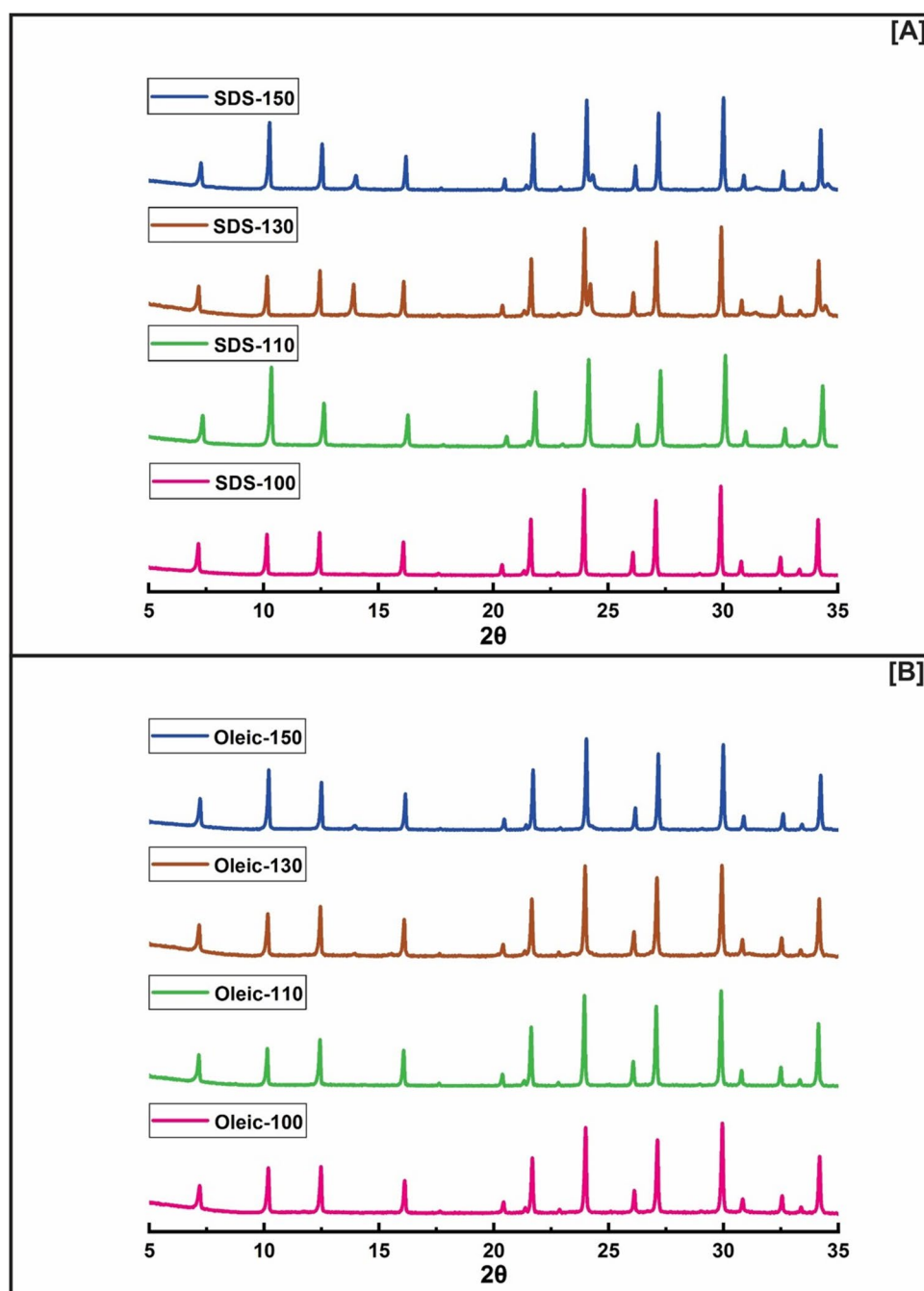
samples, an IR spectrometer equipped with a DTGS (deuterated triglycine sulfate) detector (model iS50 Thermo Scientific, USA) was used in the transmission mode in the 400–4000  $\text{cm}^{-1}$  spectral range. The samples were prepared by grinding calcinated zeolites with KBr to make a pellet.

## 3 Results and discussion

### 3.1 Phase identification and structure confirmation

Powder X-ray diffraction (PXRD) was carried out to identify the crystalline phases present in synthesized zeolite and their percentage crystallinity. Figures 2A, B, 3A, B and 4A, B show the PXRD diffractograms of LTA zeolites synthesized by SDS, Oleic acid, TPAB, HDAB, Triton and PEG, respectively. Clear diffraction peaks appeared at around  $2\theta = 7.20^\circ$ ,  $10.19^\circ$ ,  $12.49^\circ$ ,  $16.14^\circ$ ,  $21.72^\circ$ ,  $24.04^\circ$ ,  $26.17^\circ$ ,  $27.11^\circ$ ,  $29.94^\circ$ , and  $34.18^\circ$  corresponding to the crystal planes of (2 0 0), (2 2 0), (2 2 2), (4 2 0), (6 0 0), (6 2 2), (6 4 0), (6 4 2), (8 2 0), and (6 6 4) respectively (JCPDS number 43–142).

**Fig. 2** PXRD patterns of LTA zeolites synthesized in the presence of anionic surfactants of **A**: SDS, **B**: Oleic acid at different temperatures

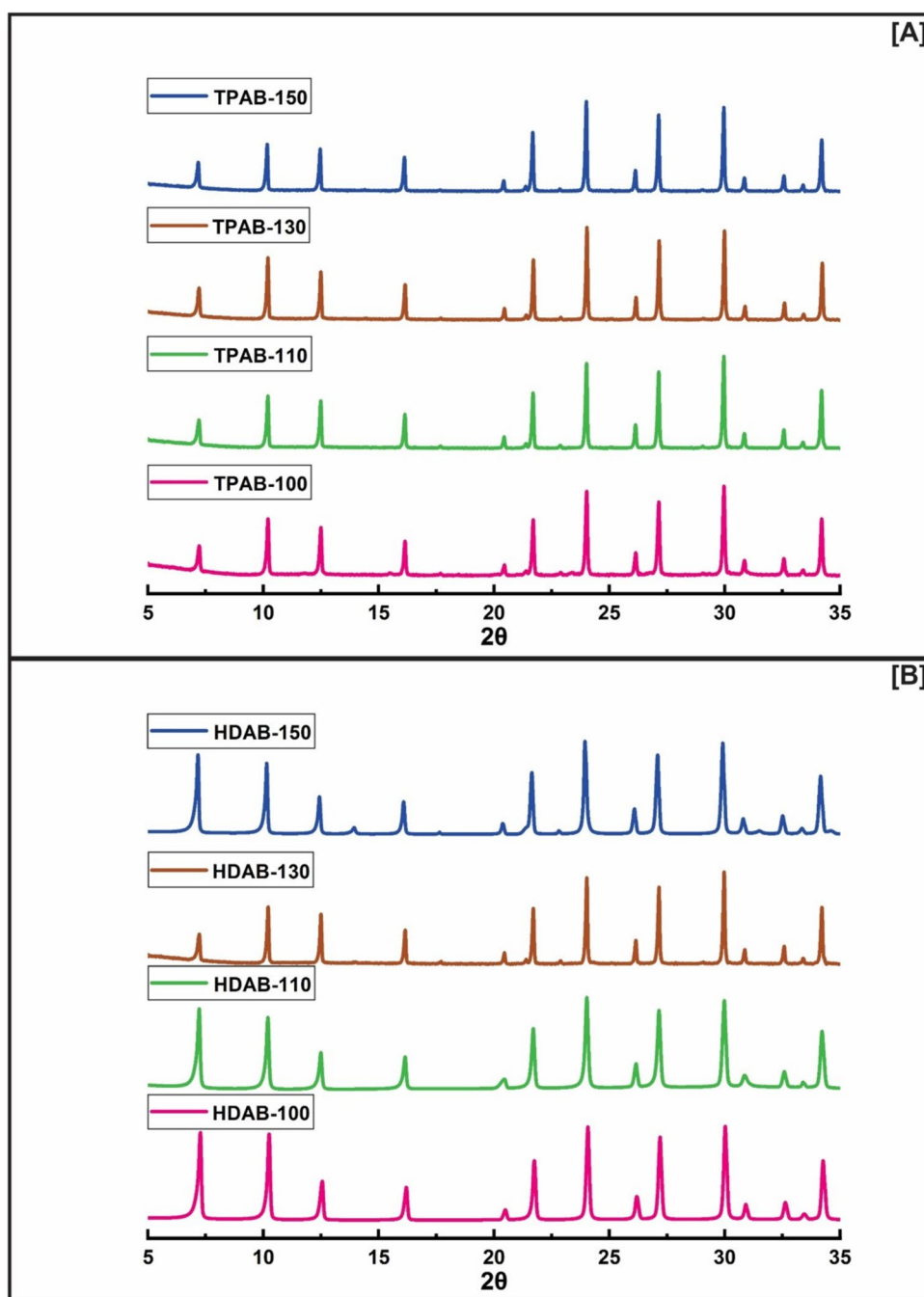


This confirms the successful formation of LTA-type zeolites in the study [21].

Raman spectra of samples prepared by using SDS, Oleic acid, TPAB, HDAB, Triton, and PEG, are shown in Figs. 5A, B, 6A, B, and 7A, B, respectively. Peaks observed around 280, 338, 410, 490, and 990  $\text{cm}^{-1}$  correspond respectively, to the bending mode of the 8-membered Si–O–T ring, bending mode of the 6-membered Si–O–T ring, 4 membered Si–O–T ring, T–O symmetric stretching from the 4-membered ring, and asymmetric T–O stretching modes. This observation further supports

the PXRD confirmation of LTA-type zeolite formation [22]. FTIR spectra of samples prepared by using SDS, Oleic acid, TPAB, HDAB, Triton, and PEG, are shown in the supporting information document (SF<sub>1</sub>–SF<sub>6</sub>). Peaks observed around 670, 1000, 1640, and 3400  $\text{cm}^{-1}$  correspond respectively, to symmetric Al–O stretches of LTA, asymmetric vibrations related to (Si, Al) O<sub>4</sub> tetrahedral (internal) of LTA, OH bending vibrations, and OH stretching vibrations (Si–OH, Si–OH–Al, H–OH) further confirm the LTA zeolite formation in all cases [20].

**Fig. 3** PXRD patterns of LTA zeolites synthesized in the presence of cationic surfactants of **A**: TPAB, **B**: HDAB at different temperatures



### 3.2 Phase purity and crystal plane preference study

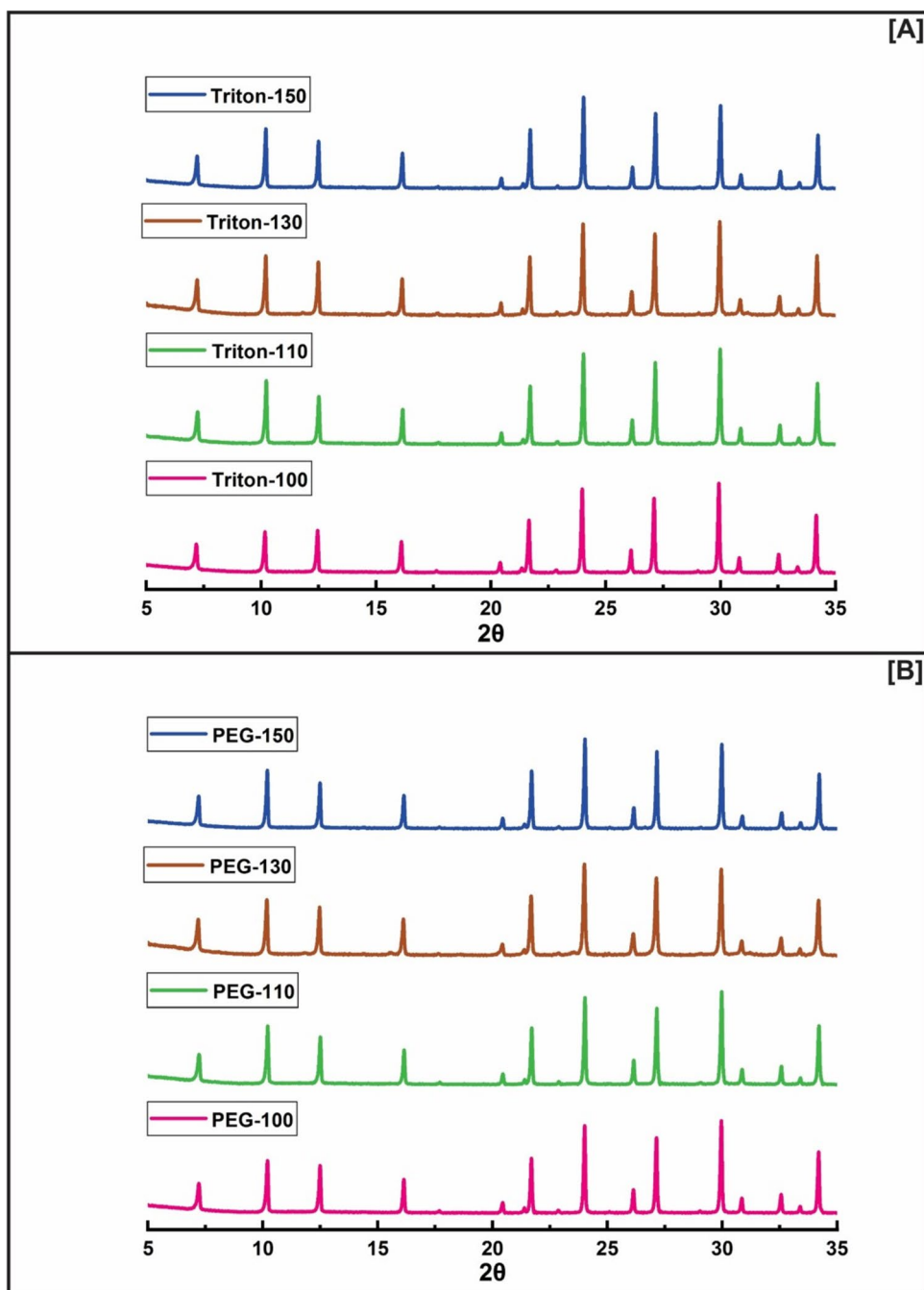
Some additional peaks with considerable intensities, which are irrelevant to the LTA phase identification, appeared in the PXRD patterns of several samples. These additional phases indicate the variation in the phase purity [23] of synthesized LTA zeolite with different surfactants and crystallization temperatures. While these peaks were not visually prominent in the diffractogram due to their low relative intensities, their presence was confirmed through careful peak data examination. Table 1 lists the impurity phases,

their relative intensities, and estimated phase purity for each sample. The overall LTA phase purity remains high (>95%) in most cases, indicating the predominance of the target phase.

LTA phase purity of each sample was calculated according to the following equations [24] (see supporting information):

$$\text{LTA phase purity} = (100 - \text{Total percentage of each impure phase})\%$$

**Fig. 4** PXRD patterns of LTA zeolites in the presence of non-ionic surfactants of **A** Triton, **B** PEG at different temperatures



% Of each impure phase =  $(a/b) \times 100\%$ ;

where a and b are the absolute intensity of the diffraction line corresponding to the particular impure phase and the sum of

the absolute intensities of all diffraction lines, respectively. Moreover, the relative crystallinity of synthesized zeolites was determined according to the following formula, using the peak area integration method [25], which separates the crystalline and amorphous contributions from the XRD pattern (Table 1).

Relative crystallinity =  $(\text{Area of crystalline peaks} / \text{total area of crystalline/amorphous peaks}) \times 100\%$

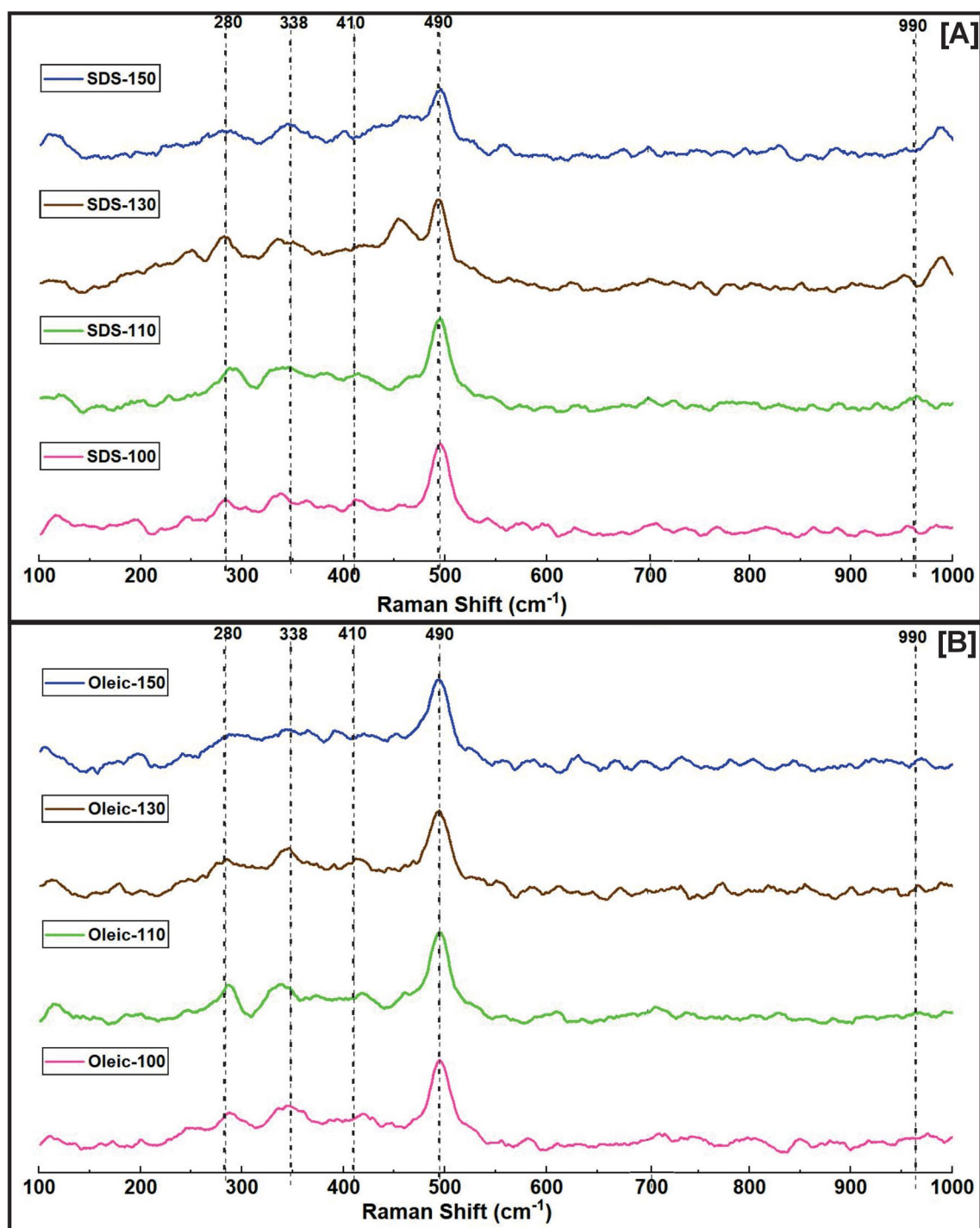


**Fig. 5** Raman spectra of LTA zeolites in the presence of anionic surfactants of **A:** SDS, **B:** Oleic acid at different temperatures

In addition to phase purity, crystal phase transitions in zeolites occurring on heating can have a considerable dependence on crystallization temperature and surfactants used in the process [26]. Crystallization temperature is a highly important parameter in the process of zeolite synthesis since its variation can affect factors such as nucleation

[27], crystal growth [28], dissolution, formation, and transformation of the precursor gel [29]. Further, the polymerization reactions between the aluminate and polysilicate anions in the precursor gel and the phase transitions of metastable phases during the zeolite crystal formations can also be affected by the crystallization temperature [30]. As well as

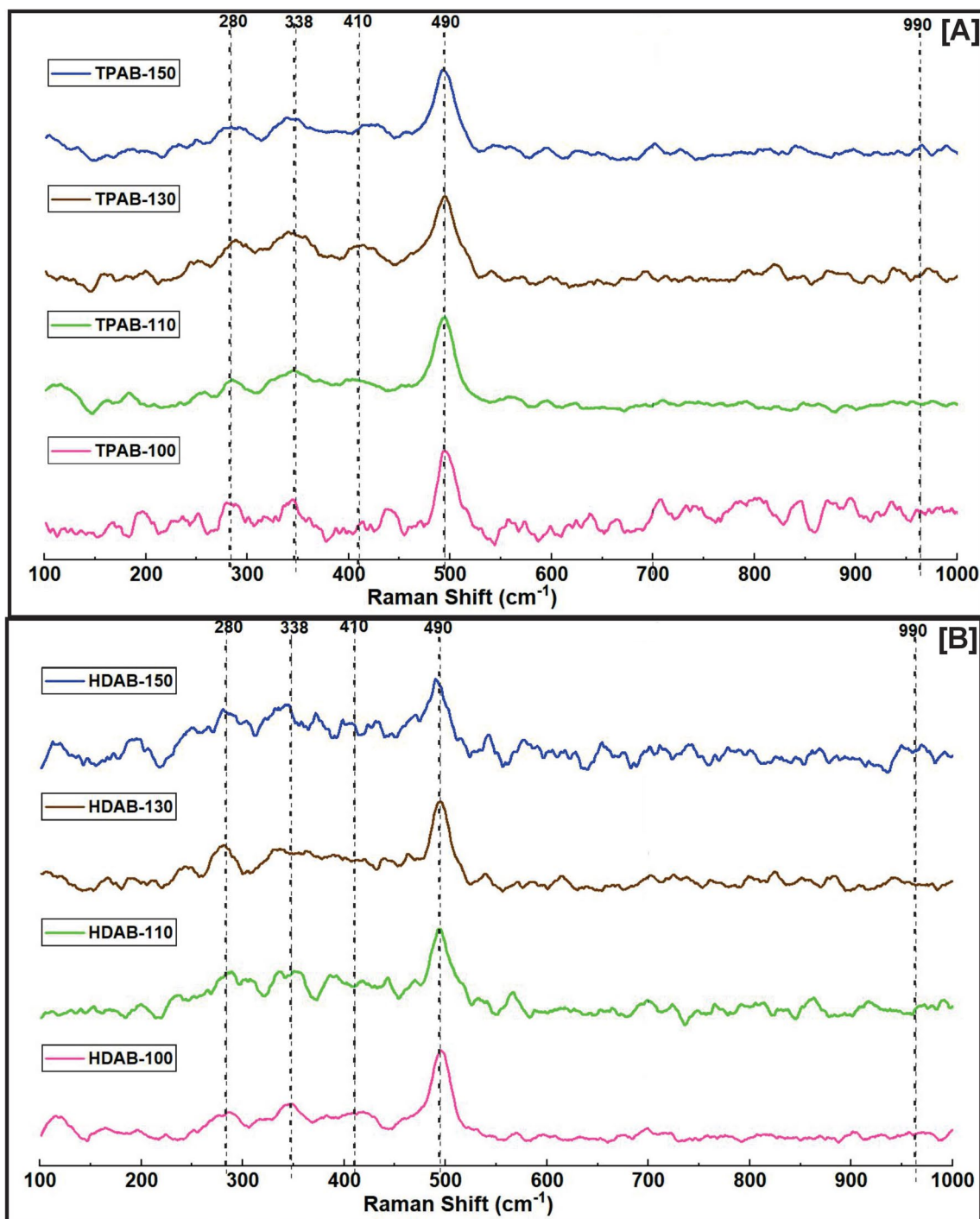


**Fig. 6** Raman spectra of LTA zeolites synthesized in the presence of cationic surfactants of **A**: TPAB, **B**: HDAB at different temperatures

the crystallization temperature, surfactants would have an involvement in the nucleation and crystallization processes [9, 31]. In this study, SEM and Raman Spectroscopy were used to investigate the possibility of phase transformations during the process of LTA zeolite crystallization in the

presence of surfactants at varying crystallization temperatures under microwave irradiation. The variation in phase purity, the possibility of phase transitions with crystallization temperature and different types of surfactants have been discussed in detail below.

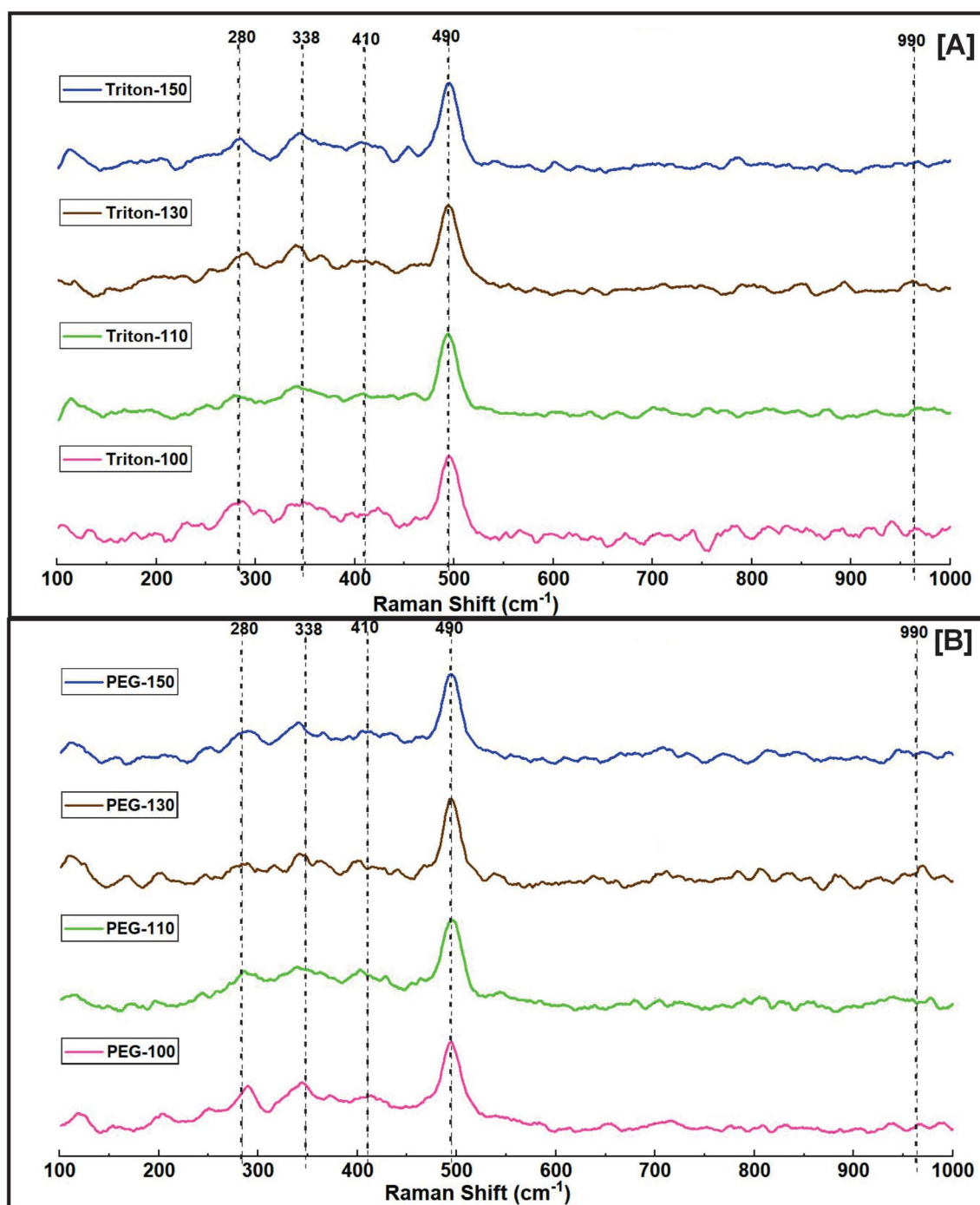


Fig. 7 Raman spectra of LTA zeolites synthesized in the presence of non-ionic surfactants of **A**: Triton, **B**: PEG at different temperatures

### 3.2.1 Effect of anionic surfactants

When considering the PXRD results of the samples synthesized in the presence of anionic surfactants (SDS and Oleic acid), the lower crystallization temperatures (100 °C and 110 °C) have resulted in LTA without any other phases and with higher crystallinity. However, with the crystallization

temperature increment (at both 130 °C and 150 °C temperatures), SDS has led to the formation of the hydroxy-sodalite phase [32]. Oleic acid has resulted in the Offretite (OFF) phase [33] at 130 °C as an additional phase. At the highest temperature of 150 °C, no other additional phases were observed. All the peak data (peak positions and their corresponding crystal planes) of synthesized zeolites are listed

**Table 1** Additional diffraction lines that were observed in the diffractograms of synthesized LTA zeolite and their percentage crystallinity. (Not defined: no relevant zeolite phase identified)

Sample name	Additional peak positions (2 $\theta$ )	Relative intensity (%)	Relevant phase identification	Impure phase %	LTA phase purity %	Crystallinity (%) of the sample
SDS-100	–	–	–	–	100	88.6
SDS-110	–	–	–	–	100	88.0
SDS-130	13.91°	33.50	Hydroxy-sodalite	6.92	93.09	80.2
	24.23°	34.00	Hydroxy-sodalite			
SDS-150	14.02°	14.70	Hydroxy-sodalite	3.05	96.95	87.9
	24.33°	15.80	Hydroxy-sodalite			
Oleic-100	–	–	–	–	100	81.1
Oleic-110	–	–	–	–	100	85.5
Oleic-130	15.53°	2.50	Not defined	0.29	99.47	80.9
	23.53°	2.00	Offretite (OFF)	0.23		
Oleic-150	–	–	–	–	100	84.4
TPAB-100	26.75°	3.00	Moganite/Keatite	0.34	98.92	82.9
	15.49°	2.10	Weinebeneite (WEI)	0.23		
	11.76°	1.10	LTL	0.12		
	18.46°	1.40	Liottite	0.15		
	23.38°	2.20	Not defined	0.25		
TPAB-110	–	–	–	–	100	87.8
TPAB-130	–	–	–	–	100	89.0
TPAB-150	–	–	–	–	100	88.8
HDAB-100	–	–	–	–	100	
HDAB-110	–	–	–	–	100	
HDAB-130	13.99°	1.3	Hydroxy-sodalite	0.25	99.07	86.7
	17.70°	2.8	Gmelinite (GME)	0.30		
	22.89°	3.4	Epistilbite (EPI)	0.37		
HDAB-150	13.94°	9.4	Hydroxy-sodalite	0.63	98.73	
	17.64°	1.3	Gmelinite (GME)	0.27		
	22.81°	2.2	Epistilbite (EPI)	0.37		
Triton-100	–	–	–	–	100	80.9
Triton-110	–	–	–	–	100	88.6
Triton-130	15.60°	2.00	Faujasite ASU-7 (ASV)	0.22	99.55	83.8
	23.45°	2.10	Faujasite ASU-7 (ASV)	0.23		
Triton-150	–	–	–	–	100	87.3
PEG-100	–	–	–	–	100	78.0
PEG-110	–	–	–	–		86.2
PEG-130	11.82°	1.4	Faujasite (FAU)	0.40	99.26	86.3
	15.60°	2.3	Faujasite (FAU)			
	23.45°	3.0	Faujasite ASU-7 (ASV)	0.34		
PEG-150	–	–	–	–	100	88.9

in ST<sub>1</sub>-ST<sub>6</sub> tables in the supporting information document. Further, the relative intensities of the diffraction lines corresponding to the hydroxy-sodalite phase at 150 °C are considerably lower than those at 130 °C (Table 1).

Therefore, it can be suggested that the intermediate temperature of 130 °C has the highest effect on the formation of impure phases in the process of LTA crystallization in the presence of these two anionic surfactants, resulting in the

lowest crystallinity values for the synthesized LTA zeolite. At lower temperatures, the kinetics of the crystallization process are relatively slower. This allows for more controlled and gradual nucleation and growth of LTA zeolite crystals. The slower kinetics at lower temperatures favor the formation of a pure LTA phase because there is sufficient time for the precursor molecules to arrange themselves in the desired crystal structure. The higher crystallinity observed is a result

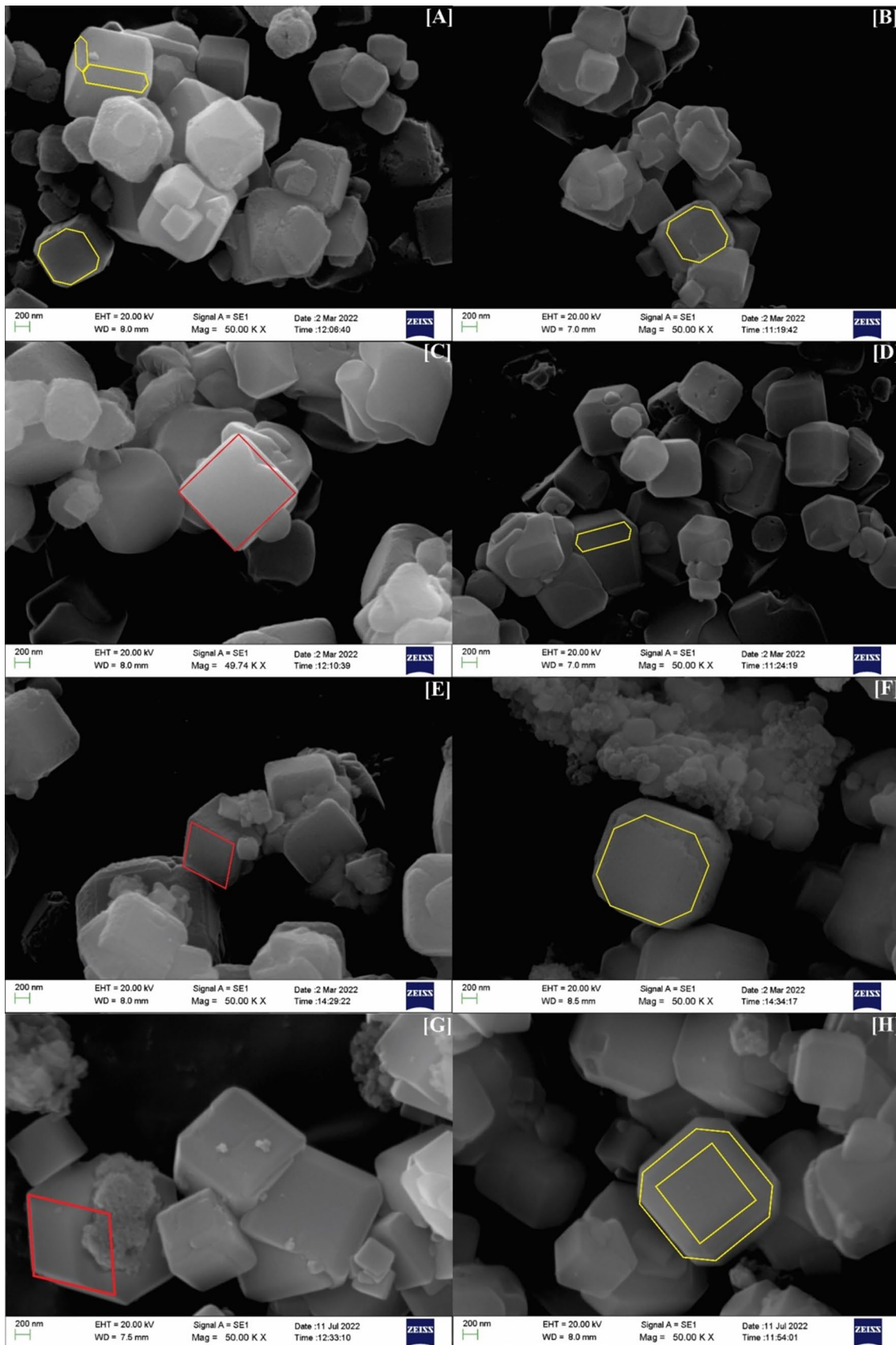


**Fig. 8** SEM images of zeolites synthesized in the presence of SDS; **A:** at 100 °C, **B:** at 110 °C, **C:** at 130 °C, **D:** at 150 °C and Oleic acid; **E:** at 100 °C, **F:** at 110 °C, **G:** at 130 °C, **H:** at 150 °C

of the orderly and more uniform growth of LTA crystals under these conditions. As the temperature increases, the kinetic energy of the molecules in the reaction mixture also increases leading to faster nucleation and growth of crystals [34], but they can also result in less control over crystal formation [35]. At 130 °C, the anionic surfactant SDS promotes the formation of the hydroxy-sodalite phase as an impurity. This may be due to the surfactant's unexpected interaction with the precursor molecules, leading to a different crystal structure, that would further need to be understood through deep studies of their mechanisms. However, at 150 °C, the higher temperature might disrupt the mechanism that leads to the formation of the hydroxy-sodalite phase, thereby inhibiting the impurity's formation indicating higher energy promotes the direct formation of LTA zeolite without impurities.

The intensity of diffraction peaks in PXRD analysis is directly related to the number of atoms in a specific crystal plane and their arrangement. PXRD quantitative analysis by peak intensity is a method used to determine the composition and quantify the amount of different crystalline phases in a sample [36]. In this study, the absolute intensities of the 10 most intense diffraction lines of LTA synthesized compared with each surfactant at 4 different temperatures to understand the growth variation of LTA characteristic crystal planes (see  $ST_8$ - $ST_{13}$  in the supporting information document). While this approach provides valuable insights, one limitation of this approach is the reliance on absolute intensities, which are influenced by variations in overall crystallinity between samples. This approach may introduce discrepancies when comparing crystal plane growth directly across different temperatures. Normalizing intensities relative to the most intense peak could provide a more accurate representation of relative growth trends. Additionally, factors such as instrumental variations and sample preparation inconsistencies may affect intensity measurements. Future work could normalize intensities to further minimize crystallinity effects. However, we believe the current findings provide meaningful insights into temperature-induced crystal growth, contributing to the understanding of crystal plane evolution.

When the absolute intensities of the 10 highest intense peaks were considered for the anionic surfactants of SDS and Oleic acid, at 130 °C both SDS and Oleic acid gave the lowest absolute intensity for all diffraction peaks. A decrease in intensity at 130 °C implies that certain crystal planes have been hindered in their formation, possibly due to surfactant interference such as adsorbing onto crystal surfaces, affecting the growth of specific crystal planes [37]. Therefore, it

can be suggested that this temperature, in conjunction with anionic surfactants, has influenced the crystal structure by potentially hindering the formation of major crystal planes. However, the highest absolute intensity of each LTA characteristic peak was observed for the sample synthesized at the lowest temperature of 100 °C in the presence of SDS, while the highest temperature of 150 °C resulted in peaks with the highest absolute intensities in the presence of Oleic acid. This suggests that the formation of LTA crystal planes accelerates at the lowest temperature (100 °C) in the presence of SDS, whereas at the highest temperatures (150 °C) in the presence of Oleic acid. At the 130 °C intermediate temperature, the formation of LTA crystal planes is lowered in the presence of both anionic surfactants [38].

As shown in Fig. 2, the diffractograms of LTA synthesized in the presence of anionic surfactants at 100 °C, 110 °C, and 130 °C crystallization temperatures, the peak appeared corresponding to the (8 2 0) crystal planes at around 29.94° predominated. However, at the highest temperature of 150 °C, the major peak corresponding to the (6 2 2) crystal plane shifted to 23.99° [39]. The shift in the major peak indicates that the temperature sensitivity of the crystal structure of LTA zeolite [40]. This suggests a temperature-driven alteration in the arrangement of atoms within the zeolite lattice with anionic surfactants. At 100 °C, 110 °C, and 130 °C, the presence of crystal plane (8 2 0) dominates, indicating a specific crystal plane preference at these temperatures. However, at 150 °C, the preference shifts towards the (6 2 2) crystal plane. These findings imply that the choice of crystallization temperature plays a crucial role in determining the preferred crystal plane and, consequently, the overall crystal structure, morphology, and properties of LTA zeolite when synthesized in the anionic surfactants' presence.

To study the morphology of crystals formed in the presence of anionic surfactants, SEM. According to the SEM images shown in Fig. 8, zeolites synthesized in the presence of SDS at all temperatures except 130 °C were predominantly regular cubic crystals. LTA crystals formed at 100 °C and 110 °C crystallization temperatures were observed as regular cubic crystals with sharp edges and apexes but at the increased temperature of 130 °C, irregular or distorted cubic forms predominated [41]. This suggests that the symmetry of the  $TO_4$  units in the LTA zeolite has been disturbed [42] to some extent (Fig. 8C) at this temperature. At elevated crystallization temperatures, the increased thermal energy disrupts the symmetry of  $TO_4$  (T = Si, Al) tetrahedral units in LTA zeolites, leading to bond length and angle distortions that affect crystal growth. This distortion creates anisotropic growth conditions, favoring certain crystal faces and resulting in morphological changes such as truncated cubic shapes at higher temperatures. The process aligns with surface energy minimization principles, where higher temperatures promote the growth of facets that reduce internal stress and

overall surface energy. Studies on zeolite A and W have shown similar temperature-dependent growth mechanisms, supporting the link between thermal-induced framework distortion and altered crystal morphology [28, 43, 44].

According to the Raman spectra of the SDS-130 sample, as shown in Fig. 5A, the appearance of an additional peak at around  $471\text{ cm}^{-1}$  can be attributed to the symmetry disturbance [45] because it may have interfered with the typical band corresponding to the  $\text{TO}_4$  stretching vibrations at  $490\text{ cm}^{-1}$  [22]. Further, the comparatively decreased crystallinity (Table 1) also supports this observation which may have introduced defects and disrupted the crystal structure (to be discussed later under the crystal defect study). However, this symmetry change cannot be directly attributed to a phase transition because there is no supporting evidence for LTA phase transitions at this temperature. Therefore, it can be suggested that the process has not gone to a new stable phase properly but to a metastable phase. In zeolite synthesis, a stable phase corresponds to the thermodynamic minimum, where the system's Gibbs free energy ( $\Delta G$ ) is at its lowest for given conditions, indicating maximum thermodynamic stability. Conversely, a metastable phase exists at a local, but not global, minimum of Gibbs free energy, meaning it has higher  $\Delta G$  compared to the stable phase but remains kinetically trapped in this state [46, 47]. Phase transformation in zeolite structure with increasing temperature can be explained by the Ostwald rule of stages, a phenomenon where kinetic pathways lead to the initial formation of a thermodynamically metastable structure that undergoes a series of recrystallization steps to form structures with progressively higher stability. These transformations occur through the gradual dissolution of one phase with the simultaneous nucleation and growth of a second (more stable) phase [48]. In the SEM image of the SDS-150 zeolite sample, again, the predominance of cubic crystals with sharp edges and apexes was observed. Therefore, according to the above explanation, we can propose that, when the crystallization temperature increases from  $130\text{ }^\circ\text{C}$  to  $150\text{ }^\circ\text{C}$ , the metastable phase gradually dissolves and nucleation occurs to produce the proper LTA zeolite stable phase [49]. The free energy diagram in Fig. 9 demonstrates how the formation of LTA zeolite at different temperatures results in either a metastable or stable phase. At  $130\text{ }^\circ\text{C}$ , the system reaches a metastable LTA phase, which sits at a local free energy minimum. Although this phase exhibits crystallinity, it retains higher internal stress and defects compared to the stable phase. Upon increasing the crystallization temperature to  $150\text{ }^\circ\text{C}$ , the system overcomes the energy barrier and reaches a lower global free energy minimum, forming stable LTA with reduced defects and sharper crystal morphology.

In contrast to SDS, the other anionic surfactant, Oleic acid, at both lower temperatures of  $100\text{ }^\circ\text{C}$  and  $110\text{ }^\circ\text{C}$ , has synthesized LTA zeolites with poorly grown edges and apexes. This suggests that, even though the lower temperatures are sufficient to direct the crystallization process to the LTA phase in the presence of SDS, those temperatures are not sufficient in the presence of Oleic acid for the proper formation of LTA. However, the absence of any additional XRD line other than LTA confirms that these two materials are still composed of LTA crystals, though they are not perfectly grown. At increased crystallization temperatures ( $130\text{ }^\circ\text{C}$  and  $150\text{ }^\circ\text{C}$ ), edges and apexes have grown well, and crystal surfaces have smoothed. In the Oleic-150 sample, an 8-membered crystal structure was observed; however, at the  $130\text{ }^\circ\text{C}$  temperature, LTA crystals in between 6-membered and 8-membered crystal structures were observed.

When the Raman spectra of these LTA zeolites are considered, a peak that corresponds to  $\text{TO}_4$  stretching vibrations at around  $490\text{ cm}^{-1}$  was broadened in the Oleic-130 and Oleic-150 spectra, and this can be attributed to the presence of 6-membered and 8-membered crystal structures in the Oleic-130 and Oleic-150 samples because their stretching frequencies are very close to each other and can overlap and cause peak broadening [50]. Other than the peak broadening, there are no considerable changes in the Raman spectra of the samples were observed, suggesting that no phase transitions occurred at these temperatures in the presence of Oleic acid [51]. Therefore, it is clear that in the presence of both of these anionic surfactants, LTA zeolite crystallization does not undergo any stable phase transitions at  $100$ ,  $110$ ,  $130$ , and  $150\text{ }^\circ\text{C}$  under microwave irradiation.

### 3.2.2 Effect of cationic surfactants

Figure 3 depicts the PXRD patterns of LTA synthesized in the presence of cationic surfactants A: TPAB and B: HDAB at different temperatures. Similar to the appearance of diffraction signals for the anionic surfactants (Fig. 2), the signals due to LTA zeolites also appeared at  $2\theta = 7.20^\circ$ ,  $10.19^\circ$ ,  $12.49^\circ$ ,  $16.14^\circ$ ,  $21.72^\circ$ ,  $23.99^\circ$ ,  $26.17^\circ$ ,  $27.11^\circ$ ,  $29.94^\circ$ , and  $34.18^\circ$ . This indicates that the LTA zeolite was formed even in the presence of cationic surfactants. It has also been noted that some additional diffraction signals appeared in the PXRD patterns (Table 1). Further, in the presence of these two cationic surfactants, a contradictory observation has resulted. LTA synthesized at a lower crystallization temperature ( $100\text{ }^\circ\text{C}$ ) in the presence of TPAB resulted in LTA with impure phases namely, Moganite/Keatite/Liottite, Weinebeneite (WEI), LTL, and Liottite/Afghanite (AFG), LTA synthesized at higher temperatures ( $130\text{ }^\circ\text{C}$  and  $150\text{ }^\circ\text{C}$ ) in the presence of HDAB has resulted in additional peaks

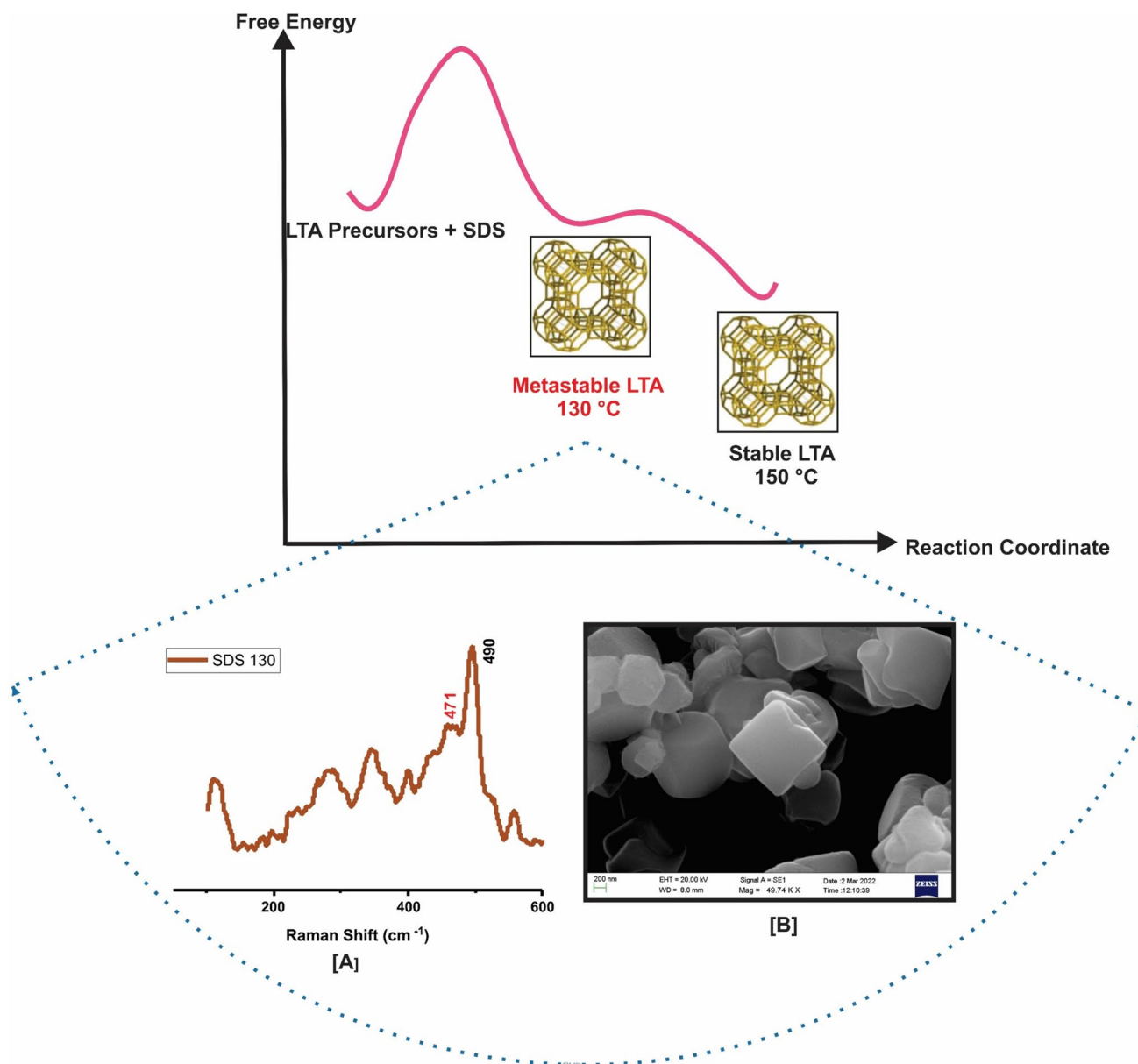


**Fig. 9** Proposed kinetic pathway for the LTA stable phase formation at 150 °C through a metastable phase at 130 °C: **A** Raman Spectrum of SDS-130 and **B** SEM image of SDS-130

corresponding to hydroxy-sodalite, Gmelinite (GME), Epistilbite (EPI) [21].

The observed differences in the impurity phases of LTA zeolite synthesized in the presence of the two cationic surfactants at varying crystallization temperatures can be attributed to the distinct characteristics of the alkyl chains present in these surfactants. TPAB and HDAB have different alkyl chain lengths. TPAB has shorter propyl chains while HDAB has longer hexadecyl chains. The alkyl chains in surfactants play a crucial role in zeolite crystallization. The hydrophilic part of the surfactant promotes crystallization, while the long hydrophobic chains inhibit crystal growth, leading to

distinct outcomes [52]. Therefore, according to the observed results, it can be proposed that shorter alkyl chains may lead to impure phases at lower temperatures, while longer chains at higher temperatures can result in different impurity phases at the tested conditions. When LTA is synthesized in the presence of cationic surfactant TPAB at lower temperatures (100 °C and 110 °C), it predominantly exhibits major crystalline planes (8 2 0). However, as the crystallization temperature increases, a shift to major planes of (6 2 2) is observed. This behavior is similar to what's observed with anionic surfactants and indicates that TPAB, a cationic surfactant, influences the choice of major crystalline planes depending on

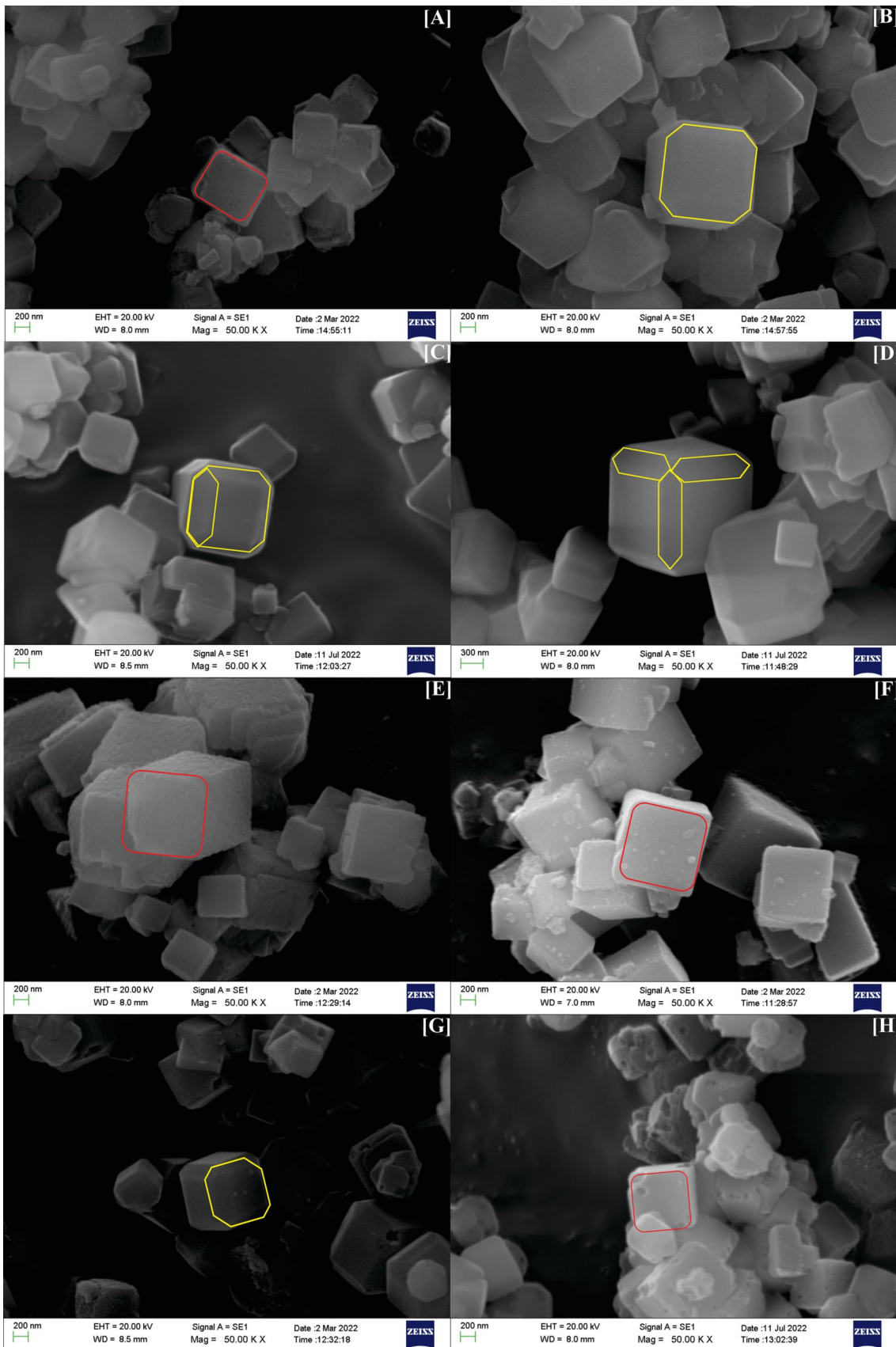


**Fig. 10** SEM images of zeolites synthesized in the presence of TPAB; **A:** at 100 °C, **B:** at 110 °C, **C:** at 130 °C, **D:** at 150 °C and HDAB; **E:** at 100 °C, **F:** at 110 °C, **G:** at 130 °C, **H:** at 150 °C

microwave temperature. In contrast, when HDAB is present, there is minimal variation in the major crystalline planes was observed, suggesting a consistent effect across temperatures used in this study. Notably, LTA synthesized at 100 °C in the presence of TPAB shows the lowest absolute intensities of major diffraction peaks, indicating that 100 °C may not be conducive for the formation of characteristic LTA planes with this cationic surfactant. On the other hand, both 130 °C and 150 °C result in the highest absolute intensities, signifying that these temperatures are more favorable for LTA plane formation when cationic surfactants are present.

According to the SEM images shown in Fig. 10, zeolite materials synthesized in the presence of cationic surfactants exhibited a strong correlation with the PXRD results, providing valuable insights into the influence of different surfactants and crystallization temperatures on zeolite crystal morphology. In the case of TPAB-100, the crystals displayed a cubic shape. However, their surfaces were notably rough, and the edges and apexes were deeply truncated. This suggests that a lower crystallization temperature is unfavorable for achieving well-developed LTA crystals in TPAB's presence. As the temperature increased to 110 °C, 130 °C, and 150 °C, the crystals' morphology improved, with sharper edges and apexes, indicating that TPAB promoted the formation of well-defined LTA crystals with temperature increment. Raman spectroscopy results can provide further insights into any phase transitions in this context.

In contrast, the HDAB-100 and HDAB-110 samples exhibited poorly developed LTA zeolite crystals. The SEM images of HDAB-100 showed the absence of 6- and 8-membered structures, featuring only 4-membered cubes with rough surfaces, truncated edges, and apexes. At 110 °C, there was a modest improvement in morphology, with somewhat sharper edges on the cubes, though surface imperfections persisted. The HDAB-130 sample, synthesized at 130 °C, exhibited well-formed cubic LTA crystals (8-membered) with properly developed edges and apexes. This suggests that 130 °C remains favorable for LTA crystal formation, despite the emergence of additional PXRD peaks corresponding to other zeolite phases, without significantly affecting LTA crystal quality. However, at the highest crystallization temperature of 150 °C, damaged LTA cubes were predominant in the SEM images, indicating that the formation of additional crystal phases adversely impacted LTA crystal growth at this elevated temperature in the presence of HDAB.

In the Raman spectra of LTA synthesized in the presence of cationic surfactants (Fig. 6), there was no observable trend of peak broadening. Further, any additional peaks

other than the characteristic peaks of LTA zeolite did not appear. Therefore, it can be concluded that in the presence of both of these cationic surfactants, LTA zeolite crystallization does not undergo any stable phase transitions or any metastable phases at 100, 110, 130, and 150 °C under microwave irradiation.

### 3.2.3 Effect of non-ionic surfactants

Figure 4 shows the PXRD patterns of LTA zeolites synthesized in the presence of non-ionic surfactants A: Triton and B: PEG at different temperatures. As with anionic and cationic surfactants, the formation of LTA zeolite was confirmed. In addition, the resulting LTA zeolite materials exhibited the formation of impure phases when subjected to an intermediate crystallization temperature of 130 °C. Both Triton and PEG samples exhibited the presence of Faujasite (FAU), where Triton led to ASV phases and PEG resulting in ASU-7 (ASV) phases [21]. Moreover, the primary crystalline phase predominantly appeared as (8 2 0) at lower crystallization temperatures, specifically at 100 °C and 110 °C. As the temperature increased to 130 °C and 150 °C, a transition to the major crystalline plane (6 2 2) was observed.

The variation in the absolute intensity of the major LTA peak with temperature in the presence of non-ionic surfactants closely resembled the trend observed with cationic surfactants, differing from that of anionic surfactants. Notably, at the intermediate temperature of 130 °C, the absolute intensities of LTA characteristic peaks were at their lowest for samples synthesized in the presence of Triton and PEG. In contrast, the highest intensity was observed at both the highest temperature of 150 °C and the lowest temperature of 100 °C. This indicates that LTA crystal plane formation is promoted at both extreme temperature ends, while the intermediate temperature significantly suppresses LTA crystal plane formation in the presence of non-ionic surfactants.

These findings are further corroborated by SEM results (Fig. 11). LTA zeolite crystals synthesized at 100 °C and 150 °C exhibited typical 8-membered cubic crystals with well-developed edges and apexes when Triton and PEG were employed. However, SEM images of Triton-130 and PEG-130 showed the presence of only 4-membered cubes, aligning with the PXRD results that highlight the unfavorable nature of 130 °C for LTA formation in the presence of non-ionic surfactants. Furthermore, Triton-110 and PEG-110 images predominantly displayed 8-membered LTA cubes, albeit with comparatively rough surfaces and less distinct edges. This implies that increasing the crystallization temperature from 100 °C to 150 °C may have led to phase transitions or the presence of metastable phases at 110 °C and 130 °C when Triton and PEG non-ionic surfactants are

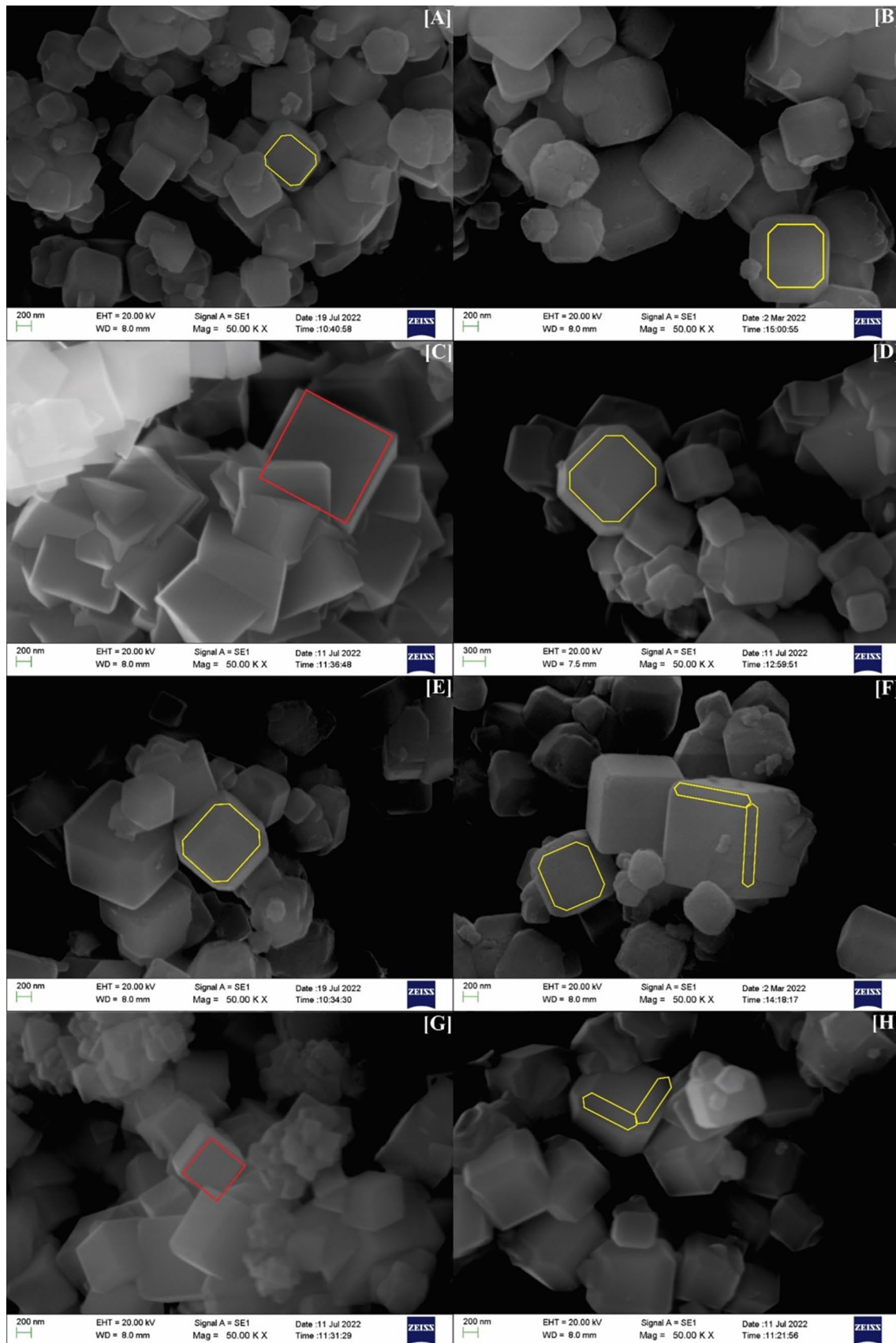


**Fig. 11** SEM images of zeolites synthesized in the presence of Triton; **A:** at 100 °C, **B:** at 110 °C, **C:** at 130 °C, **D:** at 150 °C and PEG; **E:** at 100 °C, **F:** at 110 °C, **G:** at 130 °C, **H:** at 150 °C

used. However, further confirmation was needed. Therefore, Raman spectroscopic characterization results we analyzed.

In the corresponding Raman spectra (Fig. 7), there was no observable trend of peak broadening. Further, any additional peaks other than the characteristic peaks of LTA zeolite did not appear except the peak at  $470\text{ cm}^{-1}$  in the Raman spectrum of Triton-150. However, the interference of this peak with the typical band corresponding to the  $\text{TO}_4$  stretching vibrations at  $490\text{ cm}^{-1}$  is negligible (no considerable symmetry disturbance) since Triton-150 exhibited typical 8-membered cubic crystals with well-developed edges and apexes as well as smooth crystal surfaces in its SEM images. Therefore, it can be concluded that in the presence of both of these non-ionic surfactants, LTA zeolite crystallization does not undergo any stable phase transitions or any metastable phases at 100, 110, 130, and 150 °C.

### 3.3 Microstructural and crystal defects study

#### 3.3.1 Average crystallite size

Crystals are not able to become perfect since they do not expand to infinity in all dimensions, which produces XRD peaks instead of XRD lines. Therefore, no ideally perfect crystals exist due to their finite size, which causes broadening of the XRD lines. The main characteristics of crystalline materials extracted from the XRD peak intensity, width, and peak position ( $2\theta$ ) shifts are crystallite size and lattice strain. The size of the coherently diffracting domains is known as the crystallite size, and the average crystallite size of crystalline materials is calculated by Debye Scherrer's formula,  $D = k\lambda/\beta \cos \theta$ , where  $D$  is the average crystallite size,  $\lambda$  is the wavelength of the X-ray ( $\lambda = 0.154184\text{ nm}$ ),  $\beta$  is the full width at half maximum (FWHM) after correcting for instrumental peak broadening ( $\beta$  expressed in radians),  $\theta$  is Bragg's angle, and  $k$  is the Scherrer constant [53]. In this study, the average crystallite size was calculated using the Scherrer equation.

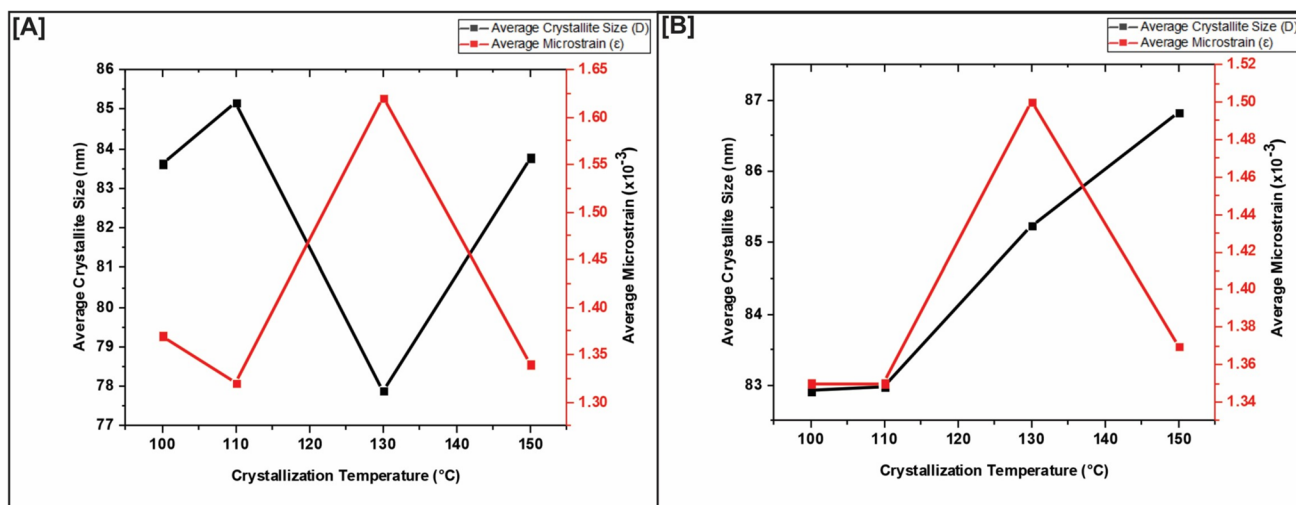
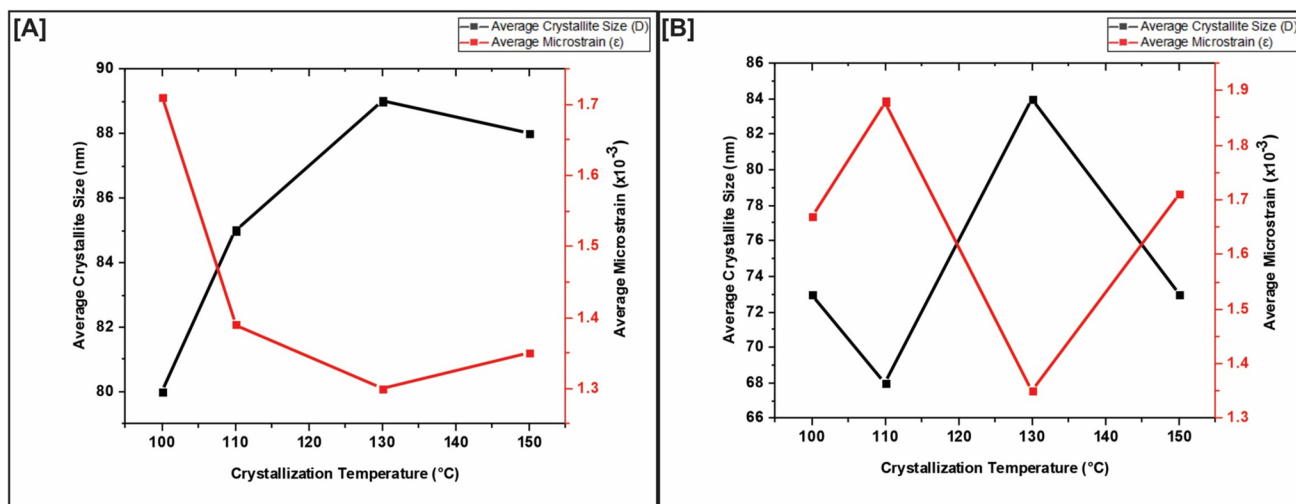
Generally, low crystallization temperatures are favored for nucleation over crystal growth and encourage the formation of crystals with a smaller crystallite size. At higher crystallization temperatures, individual nano-crystals aggregate and cause the steady congregated agglomerates to form. This can be attributed to the dominant nucleation during crystallization due to much slower crystal growth kinetics and diffusion rates at lower crystallization temperatures [54]. Surfactants are employed in the zeolite crystallization process, minimize the Ostwald ripening, and facilitate a decrease in the crystallite size [55]. When dissolved in water, surfactants

such as SDS form micelles, which are found to be slightly compressed (oblate ellipsoids), and with increasing temperature, their sizes tend to shrink, which facilitates the formation of crystals with smaller crystallite sizes. However, some surfactant molecules remain homogeneously mixed in water without participating in micelle formation [56]. The amount of this fraction is different for each surfactant, and this can be the reason for the variations in the average crystallite size of zeolites with different types of surfactants at crystallization temperature variation.

Table 2 contains the average crystallite size of LTA zeolites at 4 different crystallization temperatures. The average crystallite size variation with increasing crystallization temperature is presented in Figs. 12, 13, and 14 respectively for zeolites synthesized in the presence of anionic, cationic, and non-ionic surfactants. However, the obtained average crystallite sizes of each sample are fundamentally different from the particle size observed in SEM images, which can represent agglomerates of multiple crystallites. In this study, while SEM images reveal larger particle sizes due to agglomeration, the XRD analysis accurately reflects the average size of individual crystallites within those particles. Both measurements are crucial for a comprehensive understanding of the material properties. Following the general tendency of crystallite size variation with temperature, the average crystallite size of zeolites in the presence of the surfactants Oleic acid and Triton increased with increasing crystallization temperature. This can suggest that in this temperature range, there is no significant effect of a higher crystallization temperature on the micelle formation of Oleic acid and Triton. However, in the case of SDS, PEG, and HDAB, a remarkable change in  $D$  could be observed at a temperature of 130 °C. Zeolites synthesized at other temperatures (except 130 °C) had higher  $D$  values, and those synthesized at 130 °C in these anionic and non-ionic surfactants showed a lower  $D$  value in the presence of SDS and PEG. That can be attributed to the decrease in micelle volume with increasing temperature up to 130 °C. However, increasing the average crystallite size of zeolites formed at a further increased temperature of 150 °C may be due to an increased surfactant fraction that does not participate in micelle formation. In contrast, zeolite synthesized in the presence of HDAB cationic surfactant at this intermediate temperature of 130 °C has led to an increase in the average crystallite size when compared with the other 3 temperatures. This may be due to the crystal agglomeration at this intermediate temperature, which could not be overcome with the micelle formation by HDAB (due to the bulky alkyl groups) and may have been affected by the additional crystal phase formation at this particular temperature. However, the further increase in temperature to 150 °C has induced the lowering of the micelle size of HDAB and thus lowered the average crystallite size of zeolite. Moreover, in the presence

**Table 2** Average crystallite size and average microstrain of LTA zeolites at four different crystallization temperatures

Surfactant	SDS		Oleic acid		TPAB		HDAB		Triton		PEG	
	D (nm)	$\epsilon \times 10^{-3}$	D (nm)	$\epsilon \times 10^{-3}$	D (nm)	$\epsilon \times 10^{-3}$	D (nm)	$\epsilon \times 10^{-3}$	D (nm)	$\epsilon \times 10^{-3}$	D (nm)	$\epsilon \times 10^{-3}$
100	84	1.37	83	1.35	80	1.71	73	1.67	85	1.30	86	1.27
110	85	1.32	83	1.35	85	1.39	68	1.88	86	1.31	86	1.28
130	78	1.62	85	1.50	89	1.30	84	1.35	87	1.38	85	1.55
150	84	1.34	87	1.37	88	1.35	73	1.71	89	1.30	89	1.28

**Fig. 12** Variation of average crystallite size and average microstrain of LTA zeolites with the crystallization temperature in the presence of anionic surfactants; **A** SDS; **B** Oleic acid**Fig. 13** Variation of average crystallite size and average microstrain of LTA zeolites with the crystallization temperature in the presence of cationic surfactants; **A** TPAB; **B** HDAB

of the cationic surfactant TPAB, the average crystallite size of zeolites tends to increase with the crystallization temperature, but at the highest temperature of 150 °C, the D value

was lower than that of zeolite at 130 °C. That means that, though the presence of TPAB does not significantly affect the crystallite size at 100, 110, and 130 °C, the micelle size

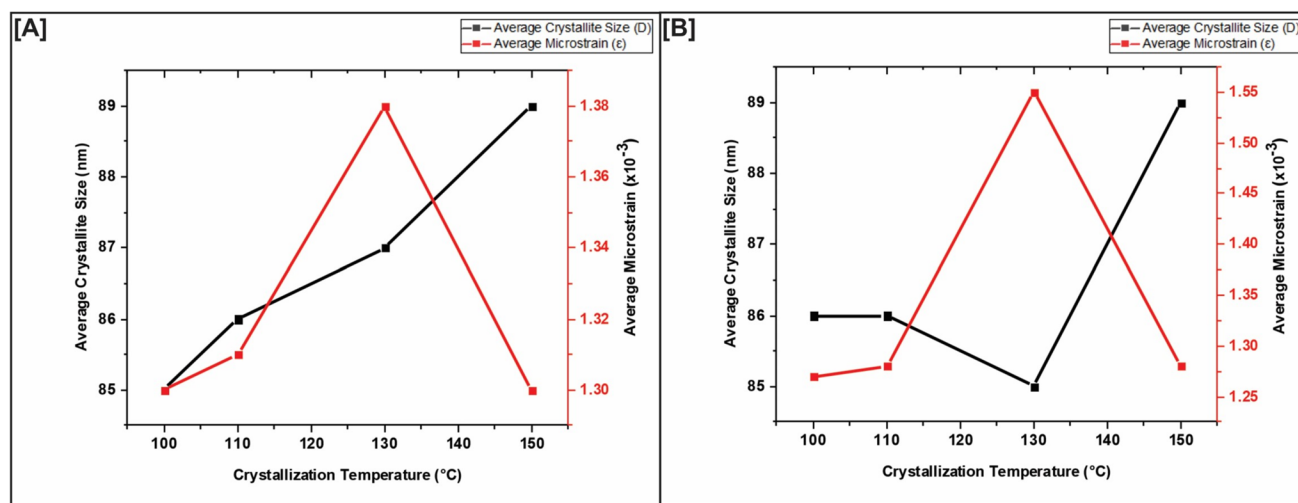


**Fig. 14** Variation of average crystallite size and average microstrain of LTA zeolites with the crystallization temperature in the presence of non-ionic surfactants; **A** Triton; **B** PEG

of TPAB has lowered at 150 °C. Similarly in the case of the other cationic surfactant of HDAB, also lowered the average crystallite size.

### 3.3.2 Crystal defects (imperfections) study

**3.3.2.1 Average microstrain** The microstrain of crystalline materials is known as the d-spacing changes throughout the domains, which have a dependency on the internal stresses and the material elastic constants. Due to the displacement of atoms that are arranged according to their referenced lattice points and the crystal lattice defects that take place throughout the domain, microstrains occur and result in peak broadening in XRD diffractograms. In other words, lattice mismatching and misfitting are the origin of the microstrain. The microstrain of crystalline materials is expressed as  $\epsilon = \beta \cot \theta / 4$  where  $\beta$  is the full width at half maximum (FWHM) after correcting for instrumental peak broadening ( $\beta$  expressed in radians),  $\theta$  is Bragg's angle [57]. The kinetic and thermal energies of the molecules that are associated with the crystallization process of the materials cause random crystal growth, which leads an internal residual stress (compression or tension), resulting in crystal deformation during the crystallization process [53].

Table 2 contains the average microstrain of LTA zeolites at 4 different crystallization temperatures. The average microstrain and crystallite size variation with increasing crystallization temperature are presented in Figs. 12, 13, and 14, respectively for zeolites synthesized in the presence of anionic, cationic, and non-ionic surfactants. Microstrain is highly dependent on the crystallite size of materials. It generally has an inverse relationship to the crystallite size, and as a thumb rule, we can say that microstrain increases

gradually with decreasing crystallite size. This can be described as follows: When the volumes occupied by the atoms arranged in the agglomerates that form from the crystallites decrease with decreasing crystallite size, the total surface area of the crystalline material tends to increase. This can cause a decrease in the crystal plane position shift and, therefore, a reduction in the microstrain of the material. In other words, the coalescence of adjacent particles tends to decrease the free volumes at the grain boundaries and, in turn, lower the crystal defects, including the microstrain of materials [58]. According to the obtained results, this general trend has been followed by LTA zeolites synthesized with the aid of all surfactants except the anionic surfactant Oleic acid and the non-ionic surfactant Triton. When the crystallization temperature increased from 110 °C to 130 °C, the average crystallite size of zeolite synthesized with the above surfactants decreased; however, their average microstrain also decreased, following a proportional relationship with the average crystallite size. This deviation from the general trend can be due to some supplementary stress applied to the crystal lattice of zeolite at this particular temperature [59]. Moreover, the formation of additional crystal phases at this temperature of 130 °C (Table 1) can have caused crystallite cracks and contributed to this supplementary stress.

**3.3.2.2 Dislocation density** Dislocations are known as the most important type of crystal defects that may be generated due to internal stresses of crystalline materials. These are the linear imperfections that occur in the slipped planes and act as boundaries between un-slipped and slipped regions in the planes of materials. When stress is applied to the crystal domain, the formed dislocations react with a driving move-

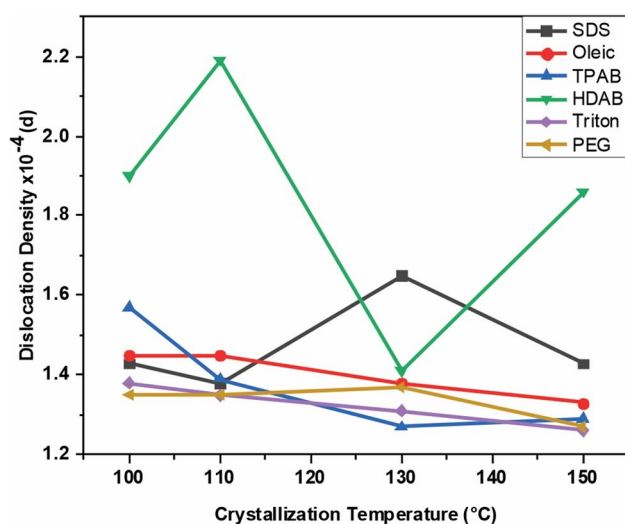


**Fig. 15** Variation of dislocation density of LTA zeolites with the crystallization temperature, synthesized in the presence of different surfactants

ment. The length of dislocation lines per unit volume of the crystal is defined as the dislocation density of materials and is known to have an important role in the rigidity, stiffness, ductility, and strength of materials [60]. Therefore, these types of defects have to be controlled. Crystallite formation, crystallite size, and the morphological features of the materials influence the dislocation density, which can be easily calculated by the Williamson–Smallman equation,  $\delta = 1/D^2$  where  $D$  is the value of the crystallite size [61].

Figure 15 depicts the dislocation density variation of LTA with the crystallization temperature for the different structure-directing agents. According to Fig. 15, it is clear that the dislocation density of zeolites varies with the crystallization temperature almost similarly in the presence of Oleic acid, TPAB, and Triton. For those zeolites, the dislocation density tends to decrease with the crystallization temperature. When compared with the other three temperatures, a sudden decrease in the dislocation density is observed in the zeolite-synthesized at 130 °C in the presence of HDAB. In contrast, a sudden increase can be observed for the zeolite synthesized at the same 130 °C temperature, in the presence of SDS interstitial vacancies [62].

The value of the dislocation density represents the vacant spaces between the crystalline clusters or crystallite agglomerations. Therefore, the decreasing value of the dislocation density can be attributed to the improvement of the crystallization process of the samples, the diminishing of the free volumes, and the reduction of the Based on this fact, it can be suggested that the intermediate temperature of 130 °C has a positive effect on the crystallization process in the presence of the cationic surfactant HDAB and a negative effect in the presence of the anionic surfactant SDS. Further, the

crystallization temperature increment has contributed to the improvement of the crystallization process in the presence of Oleic acid, TPAB, and Triton since the dislocation density has decreased in the presence of these surfactants.

## 4 Conclusions

In conclusion, PXRD, Raman, FTIR, and SEM analysis confirmed that the inclusion of any of the surfactants namely, SDS, Oleic Acid, TPAB, HDAB, Triton, and PEG in the reaction mixture does not affect crystal phase transitions between 100 and 150 °C under microwave irradiation, consistently yielding LTA-type zeolite. Interestingly, the study revealed a metastable property of the SDS-130 LTA material. However, the presence of surfactants notably influenced phase purity, crystal morphology, average crystallite size, and imperfections at particular microwave temperatures. Optimal phase purity and morphology were attained at lower temperatures (100 and 110 °C) when using anionic and non-ionic surfactants, whereas these properties were achieved at higher temperatures (130 and 150 °C) with cationic surfactants. These conclusions are supported by changes in dislocation density in HDAB-130 and SDS-130 zeolites, reflecting improvements in crystallization processes under high and low temperatures, respectively. Further, the study reveals a consistent inverse correlation between microstrain and crystallite size in LTA zeolites synthesized with various surfactants over a range of crystallization temperatures, though exceptions were observed at 130 °C. In summary, this study highlights the complex relationship between surfactants, temperature, phase purity, morphology, and crystal defects in LTA-type zeolite synthesis, calling for further exploration of crystallization mechanisms and their implications for optimizing LTA-type zeolite production. This research establishes a foundation for choosing surfactants to alter pore structures in hierarchical and mesoporous LTA zeolites, and for methodically designing LTA zeolites with tailored properties. It addresses existing knowledge gaps and sets the stage for future advances in zeolite synthesis.

**Supplementary Information** The online version contains supplementary material available at <https://doi.org/10.1007/s10934-024-01745-y>.

**Acknowledgements** This work was supported by the National Institute of Fundamental Studies (NIFS), Sri Lanka, and the National Research Council (NRC) (Grant number NRC-19-090), Sri Lanka.

**Author contributions** Dilini Perera: methodology, validation, formal analysis, investigation, visualization, writing—original draft. Lasanga Amarasena: methodology, validation, investigation, visualization. Venura Madhusanka: investigation. Xing Chen: SEM facility. Athula Bandara: methodology, validation, supervision. Rohan Weerasooriya: supervision. Lakmal Jayarathna: conceptualization, methodology, validation, supervision.

**Funding** This work was funded by National Research Council Sri Lanka, NRC-19-090.

**Data availability** No datasets were generated or analysed during the current study.

## Declarations

**Conflict of interest** The authors declare no competing interests.

## References

- C. Baerlocher, L.B. McCusker, D.H. Olson, *Atlas of zeolite framework types* (Elsevier, Amsterdam, 2007)
- E. Pérez-Botella, S. Valencia, F. Rey, Zeolites in adsorption processes: State of the art and future prospects. *Chem. Rev.* **122**(24), 17647–17695 (2022)
- Y. Li, J. Yu, Emerging applications of zeolites in catalysis, separation and host–guest assembly. *Nat. Rev. Mater.* **6**(12), 1156–1174 (2021)
- S.K. Sharma, R.V. Jasra, Review of selective production of petrochemicals through reactions in confined space of zeolites. *Catal. Green Chem. Eng.* (2022). <https://doi.org/10.1615/CatalGreenChemEng.2022041955>
- L. Bacakova et al., Applications of zeolites in biotechnology and medicine—a review. *Biomater. Sci.* **6**(5), 974–989 (2018)
- O. Larlus, V.P. Valtchev, Control of the morphology of all-silica BEA-type zeolite synthesized in basic media. *Chem. Mater.* **17**(4), 881–886 (2005)
- M. Moliner, F. Rey, A. Corma, Towards the rational design of efficient organic structure-directing agents for zeolite synthesis. *Angew. Chem. Int. Ed.* **52**(52), 13880–13889 (2013)
- E.M. Gallego et al., Simple organic structure directing agents for synthesizing nanocrystalline zeolites. *Chem. Sci.* **8**(12), 8138–8149 (2017)
- A. Sachse et al., Development of intracrystalline mesoporosity in zeolites through surfactant-templating. *Cryst. Growth Des.* **17**(8), 4289–4305 (2017)
- I. Petrov, T. Michalev, Synthesis of zeolite A: a review. *Научни трудове на русенския университет* **51**, 30–35 (2012)
- S. Minwei et al., A dynamic organic structuring-directing agent for pure-silica-zeolite AST and LTA syntheses. *Chin. J. Catal.* **33**(1), 85–91 (2012)
- J.E. Schmidt et al., The synthesis of aluminophosphate and germanosilicate LTA using a triquaternary structure directing agent. *Microporous Mesoporous Mater.* **200**, 132–139 (2014)
- K. Cho et al., Mesopore generation by organosilane surfactant during LTA zeolite crystallization, investigated by high-resolution SEM and Monte Carlo simulation. *Solid State Sci.* **13**(4), 750–756 (2011)
- Y.C. Feng et al., Synthesis of mesoporous LTA zeolites with large BET areas. *J. Porous Mater.* **20**, 465–471 (2013)
- K. Cho et al., Generation of mesoporosity in LTA zeolites by organosilane surfactant for rapid molecular transport in catalytic application. *Chem. Mater.* **21**(23), 5664–5673 (2009)
- F. Hasan et al., Direct synthesis of hierarchical LTA zeolite via a low crystallization and growth rate technique in presence of cetyltrimethylammonium bromide. *J. Colloid Interface Sci.* **382**(1), 1–12 (2012)
- R.K. Parsapur, P. Selvam, Rational design, synthesis, characterization and catalytic properties of high-quality low-silica hierarchical FAU-and LTA-type zeolites. *Sci. Rep.* **8**(1), 16291 (2018)
- H. Xin et al., Organosilane surfactant-directed synthesis of mesoporous zeolites. *Energy Environ. Focus* **2**(1), 18–40 (2013)
- I.A. Bakare et al., The effect of non-ionic surfactant in the microwave-assisted synthesis of MTT zeolite optimized by Taguchi method. *J. Taiwan Inst. Chem. Eng.* **50**, 314–321 (2015)
- I. Kannangara et al., Synthesis and characterization of nano zeolite-A with aid of sodium dodecyl sulfate (SDS) as particle size-controlling agent. *Colloids Surf. A* **589**, 124427 (2020)
- M. Treacy, J. Higgins, *Collection of Simulated XRD Power Patterns for Zeolites, 4th revised (edc.)* (Elsevier, Ameststerdam, 2001), pp.23–66
- T. Chaves et al., Monitoring of the crystallization of zeolite LTA using Raman and chemometric tools. *Analyst* **140**(3), 854–859 (2015)
- R.E. Dinnebier, S.J. Billinge, *Powder Diffraction: Theory and Practice* (Royal Society of Chemistry, London, 2008)
- Behera, P.S. and S. Bhattacharyya, Effect of processing route for preparation of mullite from kaolinite and alumina. In *AIP Conference Proceedings* (2018). AIP Publishing.
- A. Mannana et al., A method for the determination of relative crystallinity of minerals by x-ray diffraction. *Biol. Sci. PJSIR* **49**(2), 72–76 (2006)
- Emrani, P., S. Fatemi, and T.S. ASHRAF, *Effect of Synthesis Parameters on Phase Purity, Crystallinity and Particle Size of SAPO-34* (2011)
- F. Bahmanzadegan, A. Ghaemi, Modification and functionalization of zeolites to improve the efficiency of CO<sub>2</sub> adsorption: a review. *Case Stud. Chem. Environ. Eng.* (2023). <https://doi.org/10.1016/j.csee.2023.100564>
- M. Houllberghs et al., Evolution of the crystal growth mechanism of zeolite W (MER) with temperature. *Microporous Mesoporous Mater.* **274**, 379–384 (2019)
- H.J. Koroğlu et al., Effects of low-temperature gel aging on the synthesis of zeolite Y at different alkalinities. *J. Cryst. Growth* **241**(4), 481–488 (2002)
- L. Guo et al., Interzeolite conversion synthesized [Fe, Al]-FER zeolites with enhanced hydrothermal stability for NH<sub>3</sub>-SCR reaction. *Catal. Commun.* **181**, 106731 (2023)
- G. Fleury et al., Micelle formation inside zeolites: a critical step in zeolite surfactant-templating observed by Raman microspectroscopy. *ACS Mater. Lett.* **4**(1), 49–54 (2021)
- H. Greer et al., Early stage reversed crystal growth of zeolite A and its phase transformation to sodalite. *J. Am. Chem. Soc.* **131**(49), 17986–17992 (2009)
- E.-P. Ng et al., Offretite zeolite templated by amphiphile and its catalytic performance in microwave-assisted Knoevenagel condensation of benzaldehyde and ethyl cyanoacetate. *Mater. Chem. Phys.* **272**, 125001 (2021)
- Q. Li, D. Creaser, J. Sterte, An investigation of the nucleation/crystallization kinetics of nanosized colloidal faujasite zeolites. *Chem. Mater.* **14**(3), 1319–1324 (2002)
- J. Grand, H. Awala, S. Mintova, Mechanism of zeolites crystal growth: new findings and open questions. *CrystEngComm* **18**(5), 650–664 (2016)
- N. Lee, H.R. Khalid, H.-K. Lee, Synthesis of mesoporous geopolymer containing zeolite phases by a hydrothermal treatment. *Microporous Mesoporous Mater.* **229**, 22–30 (2016)
- L. Karwacki et al., Intergrowth structure of zeolite crystals as determined by optical and fluorescence microscopy of the template-removal process. *Angew. Chem.* **119**(38), 7366–7369 (2007)
- Y. Li et al., Hydrothermal stability of LTA zeolite membranes in pervaporation. *J. Membr. Sci.* **297**(1–2), 10–15 (2007)
- A. Jacas-Rodríguez et al., Mixed matrix membranes prepared from polysulfone and linde type A zeolite. *Sci. Eng. Compos. Mater.* **27**(1), 236–244 (2020)

40. A. Taherizadeh et al., Thermochemical study of the structural stability of low-silicate CHA zeolite crystals. *Results Chem.* **4**, 100466 (2022)
41. A. Shoumkova, V. Stoyanova, SEM–EDX and XRD characterization of zeolite NaA, synthesized from rice husk and aluminium scrap by different procedures for preparation of the initial hydrogel. *J. Porous Mater.* **20**, 249–255 (2013)
42. M. Serhan et al., Total iron measurement in human serum with a novel smartphone-based assay. *IEEE J. Transl. Eng. Health Med.* **8**, 1–9 (2020)
43. H.N. Kim, S.K. Lee, Temperature-induced amorphization of Na-zeolite A: a view from multi-nuclear high-resolution solid-state NMR. *Am. Miner.* **99**(10), 1996–2007 (2014)
44. Y. Zhao et al., Wulff constructions for an equilibrium MFI-type zeolite shape modelling under different conditions. *Crystals* **14**(1), 63 (2024)
45. S. Luo et al., Identifying order and disorder in double four-membered rings via Raman spectroscopy during crystallization of LTA zeolite. *Chem. Mater.* **33**(17), 6794–6803 (2021)
46. M.H. Ford, S.M. Auerbach, P. Monson, Further studies of a simple atomistic model of silica: thermodynamic stability of zeolite frameworks as silica polymorphs. *J. Chem. Phys.* **5**, 45 (2007). <https://doi.org/10.1063/1.2712440>
47. M. Moliner, Y. Román-Leshkov, A. Corma, Machine learning applied to zeolite synthesis: the missing link for realizing high-throughput discovery. *Acc. Chem. Res.* **52**(10), 2971–2980 (2019)
48. M. Maldonado et al., Controlling crystal polymorphism in organic-free synthesis of Na-zeolites. *J. Am. Chem. Soc.* **135**(7), 2641–2652 (2013)
49. A. Kumar, V. Molinero, Two-step to one-step nucleation of a zeolite through a metastable gyroid mesophase. *J. Phys. Chem. Lett.* **9**(19), 5692–5697 (2018)
50. Y.-L. Tsai et al., Raman spectroscopic characteristics of zeolite group minerals. *Minerals* **11**(2), 167 (2021)
51. N. Ovsyuk, S. Goryainov, Amorphous-to-amorphous phase transition in zeolites. *JETP Lett.* **83**, 109–112 (2006)
52. G. Rioland et al., The influence of the nature of organosilane surfactants and their concentration on the formation of hierarchical FAU-type zeolite nanosheets. *New J. Chem.* **39**(4), 2675–2681 (2015)
53. A.M. Alsaad et al., Optical, structural, and crystal defects characterizations of dip synthesized (Fe–Ni) Co-doped ZnO thin films. *Materials* **13**(7), 1737 (2020)
54. X. Zhang et al., Synthesis of NaX zeolite: influence of crystallization time, temperature and batch molar ratio  $\text{SiO}_2/\text{Al}_2\text{O}_3$  on the particulate properties of zeolite crystals. *Powder Technol.* **235**, 322–328 (2013)
55. S. Tcholakova et al., Control of Ostwald ripening by using surfactants with high surface modulus. *Langmuir* **27**(24), 14807–14819 (2011)
56. B. Hammouda, Temperature effect on the nanostructure of SDS micelles in water. *J. Res. Nat. Inst. Stand. Technol.* **118**, 151 (2013)
57. D.W. Fu et al., Diisopropylammonium chloride: a ferroelectric organic salt with a high phase transition temperature and practical utilization level of spontaneous polarization. *Adv. Mater.* **23**(47), 5658–5662 (2011)
58. A.S. Hassanien, A.A. Akl, A. Saaedi, Synthesis, crystallography, microstructure, crystal defects, and morphology of  $\text{Bi}_x\text{Zn}_{1-x}\text{O}$  nanoparticles prepared by sol–gel technique. *CrystEngComm* **20**(12), 1716–1730 (2018)
59. C. Mrabet et al., Physical properties of La-doped NiO sprayed thin films for optoelectronic and sensor applications. *Ceram. Int.* **42**(5), 5963–5978 (2016)
60. G. Williamson, R. Smallman III., Dislocation densities in some annealed and cold-worked metals from measurements on the X-ray debye-scherrer spectrum. *Phil. Mag.* **1**(1), 34–46 (1956)
61. A.A. Akl et al., Improving microstructural properties and minimizing crystal imperfections of nanocrystalline  $\text{Cu}_2\text{O}$  thin films of different solution molarities for solar cell applications. *Mater. Sci. Semicond. Process.* **74**, 183–192 (2018)
62. A.A. Akl, A.S. Hassanien, Microstructure and crystal imperfections of nanosized  $\text{CdS}_x\text{Se}_{1-x}$  thermally evaporated thin films. *Superlattices Microstruct.* **85**, 67–81 (2015)

**Publisher's Note** Springer Nature remains neutral with regard to jurisdictional claims in published maps and institutional affiliations.

Springer Nature or its licensor (e.g. a society or other partner) holds exclusive rights to this article under a publishing agreement with the author(s) or other rightsholder(s); author self-archiving of the accepted manuscript version of this article is solely governed by the terms of such publishing agreement and applicable law.